MUCOSAL IMMUNOLOGY

Bile acid–sensitive tuft cells regulate biliary neutrophil influx

Claire E. O'Leary[1], Julia Sbierski-Kind[2], Maya E. Kotas[3], Johanna C. Wagner[4]†, Hong-Erh Liang[1], Andrew W. Schroeder[1], Jeshua C. de Tenorio[5], Jakob von Moltke[6], Roberto R. Ricardo-Gonzalez[7,8], Walter L. Eckalbar[1], Ari B. Molofsky[2], Christoph Schneider[5], Richard M. Locksley[1,8,9]*

Inflammation and dysfunction of the extrahepatic biliary tree are common causes of human pathology, including gallstones and cholangiocarcinoma. Despite this, we know little about the local regulation of biliary inflammation. Tuft cells, rare sensory epithelial cells, are particularly prevalent in the mucosa of the gallbladder and extrahepatic bile ducts. Here, we show that biliary tuft cells express a core genetic tuft cell program in addition to a tissue-specific gene signature and, in contrast to small intestinal tuft cells, decreased postnatally, coincident with maturation of bile acid production. Manipulation of enterohepatic bile acid recirculation revealed that tuft cell abundance is negatively regulated by bile acids, including in a model of obstructive cholestasis in which inflammatory infiltration of the biliary tree correlated with loss of tuft cells. Unexpectedly, tuft cell–deficient mice spontaneously displayed an increased gallbladder epithelial inflammatory gene signature accompanied by neutrophil infiltration that was modulated by the microbiome. We propose that biliary tuft cells function as bile acid–sensitive negative regulators of inflammation in biliary tissues and serve to limit inflammation under homeostatic conditions.

INTRODUCTION

Bile acids (BAs) are required for uptake of fats and fat-soluble vitamins and serve as signaling molecules (*1*). Regulated excretion and concentration of bile is enabled by the gallbladder (GB) and extrahepatic bile ducts (EHBDs), a key physiologic feature in mammals with diurnal cycles of fasting and feeding (*2*, *3*). Chronic inflammation of the biliary tree promotes liver and extrahepatic biliary tissue damage (*4*–*6*), and inflammatory/obstructive biliary disease is a leading cause of liver transplant (*7*). Despite this, biliary inflammation is poorly characterized. Understanding epithelial-immune interactions in the extrahepatic biliary tree could provide important insights into common biliary pathologies.

Tuft cells are rare chemosensory epithelial cells found in many tissues (*8*) including the GB and EHBDs (*9*–*14*). Tuft cells are best characterized in the mouse small intestine, where they relay luminal signals from intestinal helminths and protists to activate lamina propria group 2 innate lymphoid cells (ILC2s), promoting differentiation of goblet cells and tuft cells themselves and adaptation of the small intestine (*10*, *15*–*18*). In other organs, tuft cells have been shown to play roles in response to allergens and bacteria (*19*–*21*) and induction of innate-like lymphocytes (*22*–*24*). GB/EHBD tuft cells express canonical tuft cell markers, including transient receptor potential cation channel subfamily M member 5 (TRPM5), interleukin-25 (IL-25), doublecortin-like kinase 1 (DCLK1), and enzymes supporting eicosanoid biosynthesis (*8*, *16*), but their physiologic role remains unknown.

We set out to characterize the tuft cell compartment of the extrahepatic biliary tree. Using bulk and single-cell RNA sequencing (scRNA-seq), together with flow cytometry and tuft cell–specific lineage-tracking and lineage-ablating tools, we describe the BA-sensitive nature of biliary tuft cells and uncover an unanticipated role for these cells in modulating the microbiome-dependent infiltration of activated neutrophils and biliary inflammatory tone.

RESULTS

Biliary tuft cells express tuft cell– and tissue-specific gene signatures

We first optimized methods in the mouse for isolation of viable epithelial, immune, and stromal cells from digested GB/EHBDs (fig. S1A). Using IL-25 reporter mice (Flare25) to identify tuft cells by flow cytometry (*10*), we found that tuft cells represented a greater percentage of epithelial cells in the biliary tree compared with small intestine (Fig. 1, A and B). As previously noted (*9*, *14*), tuft cells were present in both the GB and EHBDs by imaging of DCLK1 (fig. S1B) (*8*) and Flare25 (Fig. 1C) but absent from intrahepatic bile ducts (fig. S1C).

To assess the similarity of biliary and small intestinal tuft cells, we sorted biliary and duodenal tuft cells from Flare25 mice for bulk RNA-seq. Principal components analysis (PCA) indicated that cells clustered by tissue and tuft cell identity (Fig. 1D). Analysis of the top 1000 genes by variance across all samples (fig. S1D and table S1) revealed that biliary and small intestinal tuft cells share a core gene program, including transcripts for *Il25*, *Dclk1*, *Chat*, *Alox5*, and *Pou2f3* (Fig. 1E) (*8*). Biliary tuft cells expressed a unique signature, distinct from duodenal tuft cells and nontuft epithelial cells (Fig. 1F). Gene ontology (GO) analysis showed that biliary tuft cell–associated transcripts were enriched in genes related to axon guidance and neural development (e.g., *Robo1*, *Ascl1*, and *Sema3a*), immune-related genes

[1]Department of Medicine, University of California, San Francisco, San Francisco, CA, USA. [2]Department of Laboratory Medicine, University of California, San Francisco, San Francisco, CA, USA. [3]Division of Pulmonary, Critical Care, Allergy and Sleep Medicine, Department of Medicine, University of California, San Francisco, San Francisco, CA, USA. [4]Department of Surgery, University of California, San Francisco, San Francisco, CA, USA. [5]Institute of Physiology, University of Zurich, Zurich, Switzerland. [6]Department of Immunology, University of Washington, Seattle, WA, USA. [7]Department of Dermatology, University of California, San Francisco, San Francisco, CA, USA. [8]Department of Microbiology and Immunology, University of California, San Francisco, San Francisco, CA, USA. [9]Howard Hughes Medical Institute, Chevy Chase, MD, USA.
*Corresponding author. Email: richard.locksley@ucsf.edu
†Present address: Department of General, Visceral, Transplantation, Vascular and Pediatric Surgery, University Hospital Würzburg, Würzburg, Germany.

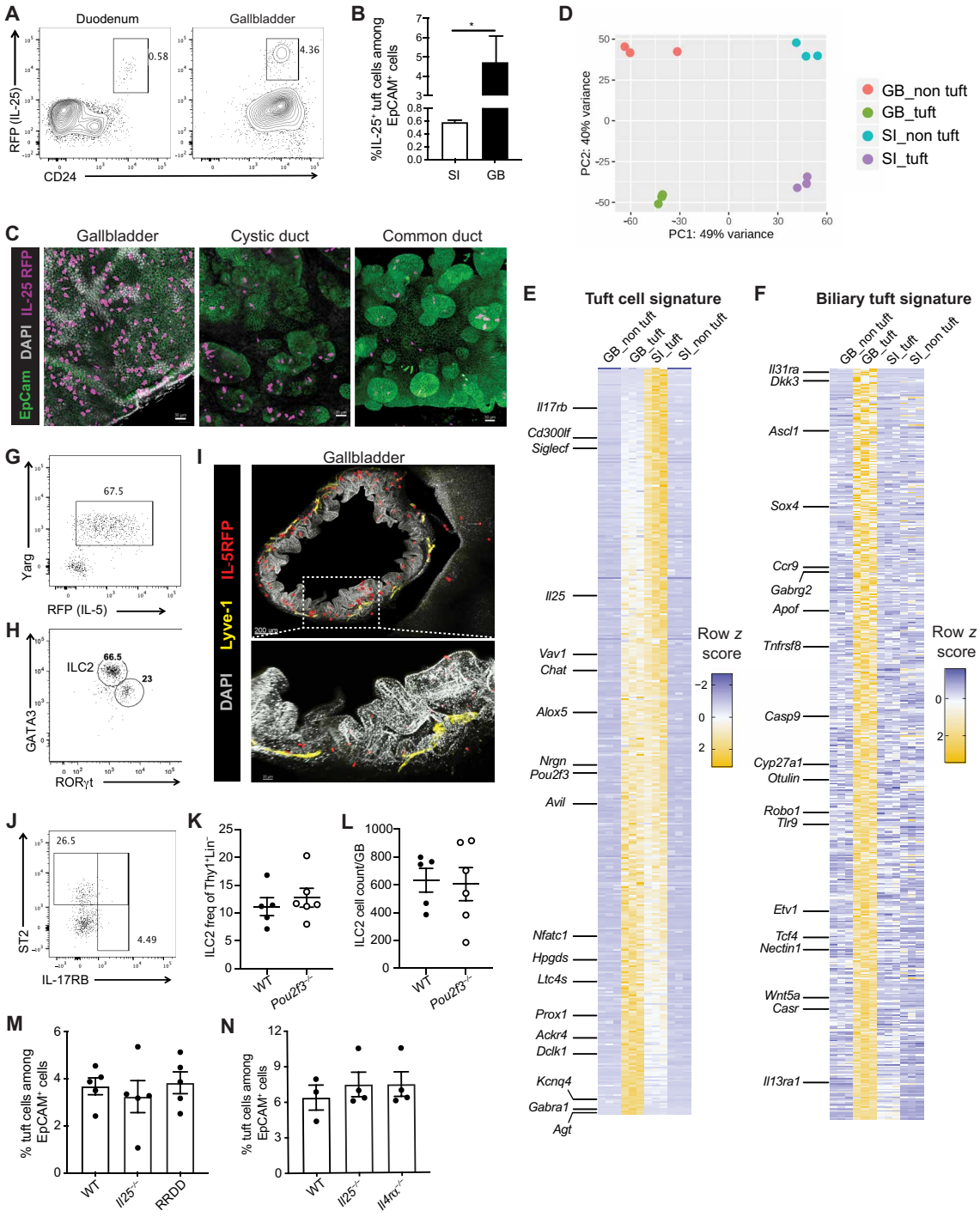

Fig. 1. Biliary tuft cells express tuft cell–specific and tissue-specific gene signature and are not dependent on type 2 cytokines. (**A** and **B**) Epithelial cells from duodenum (SI) or GB of IL-25 reporter (Flare25) mice were examined by flow cytometry. (A) Representative flow plot. Previously gated on live singlets, FSC-A × SSC-A, EpCam^{+}CD45^{-}. (B) IL-25^{+} cells as frequency of EpCAM^{+} epithelial cells from SI and GB; three mice, $^{*}P < 0.05$ by two-tailed paired *t* test. Representative of more than three experiments. (**C**). Whole-mount confocal imaging of Flare25 mouse GB, cystic duct, and common bile duct. (**D**) Tuft and nontuft epithelial cells were sorted from duodenum or GB of Flare25 mice and analyzed by RNA-seq. Unsupervised PCA of top 1000 genes by variance: biliary tuft (GB_tuft), biliary nontuft (GB_non tuft), small intestinal tuft (SI_tuft), and small intestinal nontuft (SI_non tuft). (**E** and **F**) Row *z* score for tuft cell–specific transcripts (E) and (F) biliary tuft cell–specific transcripts. (**G** and **H**) Representative flow plots. ILC2s identified in total GB/EHBD digests from arginase-1 (YARG) and IL-5 (Red5) reporter mice (G) and by transcription factor staining (H). Previously gated on live singlets, FSC-A × SSC-A, CD45^{+}lineage-Thy-1^{+},TCR-NKp46-NK1.1^{-}. (**I**) Imaging of GB and liver from Rosa$^{Ai14\text{-}RFP}$ x Red5 mice, stained for RFP (ILC2s, red), EpCAM (green), LYVE-1 (yellow), and DAPI (gray). (**J**) As in (G and H), staining for ST2 and IL-17RB on ILC2s in total GB/EHBD digest. Previously gated on live singlets, FSC-A × SSC-A, CD45^{+}lineage^{-}Thy-1^{+},TCR^{-}NKp46^{-}NK1.1^{-}YARG^{+}. (**K** and **L**) Relative frequency (K) and count (L) of ILC2s per GB/EHBD from WT and *Pou2f3*$^{-/-}$ YARG/Red5 reporter mice, as assessed by flow cytometry. (**M** and **N**) Frequency of tuft cells among biliary epithelial cells from *Il25*$^{-/-}$, ILC2-deficient (RRDD), and *Il4ra*$^{-/-}$ mice determined by flow cytometry for DCLK1.

(e.g., *Tlr9*, *Il31ra*, and *Il13ra1*), cholesterol metabolism (e.g., *Cyp27a1* and *Apof*), and WNT signaling (e.g., *Wnt5a* and *Dkk3*; fig. S1E).

Biliary tuft cell and ILC2 abundance are regulated independently

Small intestinal tuft cells make IL-25 and cysteinyl leukotrienes that drive lamina propria ILC2 function (*10*, *25*, *26*). We identified biliary resident ILC2s by flow cytometry using IL-5 [Red5; IL-5$^{tdtomato-Cre}$ (*6*)] and arginase-1 [Yarg (*27*)] reporter mice (Fig. 1G and fig. S1F) and by staining for the transcription factor GATA binding protein 3 (GATA3) (Fig. 1H). Intravenous anti-CD45 labeling confirmed tissue residency of CD45$^+$ immune cells isolated from GB/EHBDs (fig. S1G). We corroborated biliary ILC2 identity by flow cytometry analysis of *Rag1*$^{-/-}$ mice (fig. S1H) and by imaging of IL-5 lineage tracker mice (IL-5$^{tdtomato-Cre}$; Rosa26$^{RFP-A114}$) (Fig. 1I) (*28*). IL-5$^+$ lymphocytes were observed in the GB and liver, whereas tuft cells were exclusive to the extrahepatic epithelium (fig. S1I). In contrast to small intestine ILC2s, biliary ILC2s expressed suppression of tumorigenicity 2 (ST2), a component of the IL-33 receptor, but not IL-17RB, the IL-25 receptor (Fig. 1J) (*25*). Abundance of biliary ILC2s was comparable in *Pou2f3*$^{-/-}$ mice, which lack tuft cells (Fig. 1, K and L) (*29*). Consistent with this, biliary tuft cell abundance was not significantly different in mice lacking IL-25, ILC2s, or IL-4Rα compared with controls (Fig. 1, M and N), in contrast to small intestinal tuft cells, which are reduced in these strains (*10*). Together, these data suggest that factors other than type 2 cytokine signals regulate biliary tuft cells.

Biliary tuft cells are long-lived and replenish slowly in adult tissue

Biliary epithelial cells are considered quiescent, with proliferation activated by injury (*30*, *31*), but the longevity of biliary tuft cells has not been examined. We observed strong concordance between DCLK1 and IL-25/Siglec F expression among biliary tuft cells and loss of DCLK1 staining in *Pou2f3*$^{-/-}$ mice (Fig. 2A). This indicated that DCLK1 is a faithful tuft cell marker in the biliary tree, allowing us to use Dclk1$^{ERT2/+}$;R26^{YFP} (*32*) mice for tuft cell labeling. In tamoxifen-treated Dclk1$^{ERT2/+}$;R26YFP mice, we observed robust labeling and minimal decay over 6 months, suggesting that biliary tuft cells are long-lived (Fig. 2B).

To assess the recovery capacity of biliary tuft cells, we developed two *Il25* locus knock-in mouse strains, one expressing humanized Cre recombinase ("25^{Cre}"; Fig. 2C) and the other expressing tdTomato-2A-CreERT2 ("25^{ERT2}"; fig. S2A). Both retain *Il25* expression, with the latter also serving as an IL-25 reporter. To validate 25^{Cre} specificity, we generated homozygous 25$^{ERT2/ERT2}$;R26$^{YFP/YFP}$ mice and intercrossed this strain with 25$^{Cre/Cre}$ mice (25$^{Cre/ERT2}$;R26$^{YFP/+}$), generating tuft cells that coexpressed the tdTomato IL-25 reporter and were lineage traced with yellow fluorescent protein (YFP) under control of the 25^{Cre} driver (fig. S2B). Most of the IL-25$^+$ tuft cells co-expressed YFP, whereas IL-25$^-$ biliary epithelial cells were YFP negative, indicating good efficacy and specificity (Fig. 2D). Biliary tuft cells were ablated when 25$^{Cre/ERT2}$ mice were intercrossed with ROSA26–diphtheria toxin (DT) A mice (25$^{Cre/ERT2}$;R26DTA). We crossed 25$^{Cre/+}$ mice to R26 inducible DT receptor mice (25$^{Cre/+}$;R26$^{iDTR/iDTR}$) to assess recovery of biliary tuft cells after inducible DT-mediated ablation. We observed near-complete depletion of biliary tuft cells, which was sustained for 3 to 6 months after DT treatment (Fig. 2E). Thus, biliary tuft cells are long-lived and replenish slowly in adult mice.

The extrahepatic biliary epithelium expands postnatally (fig. S2C) (*33*–*35*). To compare biliary tuft cell turnover in neonatal (actively proliferating) and adult (quiescent) extrahepatic epithelium, we treated adult or postnatal day 10 neonatal 25$^{ERT2/ERT2}$;R26$^{YFP/YFP}$ mice with tamoxifen. We assessed induction of YFP in IL-25$^+$ tuft cells 24 hours after tamoxifen injection and presence of YFP$^+$ tuft cells 7 days later. Labeling efficiency was less robust than in Dclk1$^{ERT2/+}$;R26^{YFP} mice (fig. S2, D and E) but was stably retained in adult biliary tuft cells, in contrast to rapid loss from small intestinal tuft cells (Fig. 2F). YFP label was poorly retained by both biliary and small intestinal IL-25$^+$ tuft cells in neonates (Fig. 2G). IL-25$^+$ tuft cells were highly abundant before weaning and declined to adult levels around 6 weeks of age (Fig. 2H), further supporting distinct biliary tuft cell regulation in adult versus neonatal mice.

Biliary tuft cell abundance is modulated by bile acid

Weaning promotes maturation of enterohepatic recirculation (Fig. 3A), dependent on the transition from milk to solid foods and acquisition of a stable intestinal microbiota (*33*). As this coincides with the postnatal reduction of biliary tuft cell frequency, we assessed the effects of enterohepatic recirculation/BAs on tuft cells by feeding mice a 2% cholestyramine diet to sequester intestinal BAs. As expected, cholestyramine reduced small intestinal expression of the farnesoid X receptor (FXR) gene product *Fgf15*, which negatively regulates hepatic BA synthesis, thereby resulting in increased liver *Cyp7a1* expression (fig. S3A). Biliary tuft cells were almost completely eliminated in cholestyramine-fed mice compared with controls (Fig. 3B). Because cholestyramine acts indirectly to increase hepatic BA output, we tested whether the effect of cholestyramine on biliary tuft cells could be blocked by systemic activation of FXR, which would directly inhibit hepatic BA synthesis. Treatment of cholestyramine-fed mice with the FXR agonist GW4064 (*36*) sustained biliary tuft cells at normal levels (Fig. 3C). In cholestyramine-induced tuft cell loss, we observed no evidence for trans-differentiation to nontuft epithelial cells using our fate-mapping 25Cre$^{ERT/Cre}$;R26$^{YFP/+}$ mice (fig. S3B). These data suggest a role for liver BA production in the regulation of biliary tuft cell frequency.

Cholic acid (CA) is the primary BA in mice and humans (*1*), and its production is increased after cholestyramine treatment and reduced by FXR activation. Feeding 0.5% CA led to an abundance of CA in bile (fig. S3C) and resulted in rapid and near-complete elimination of tuft cells in the biliary tree (Fig. 3, D and E) but not in the small intestine (fig. S3D). Deoxycholic acid (DCA), generated by bacterial dehydroxylation of CA (*37*, *38*), was also elevated in bile after 0.5% CA feeding (fig. S3E). Supplementation of drinking water with 0.2% DCA in drinking water was sufficient to reduce biliary tuft cell frequency (Fig. 3F), suggesting a role for the microbiota in BA-induced tuft cell loss. Consistent with this, tuft cell reduction was delayed in germ-free (GF) mice fed with 0.5% CA (fig. SG), and untreated GF mice had significantly more biliary tuft cells compared with age- and sex-matched specific pathogen–free (SPF) controls (Fig. 3H).

Further implicating BAs as negative regulators of biliary tuft cell abundance, we found that frequency of tuft cells in the biliary epithelium was greatly reduced in FXR-deficient mice, which lack negative feedback on CA production in the liver (Fig. 3I) (*39*). Conversely, tuft cell frequency was unchanged in mice with CRISPR-mediated deletion of *Cyp8b1* (Fig. 3J), which is required for liver CA production (fig. S3, F and G) (*40*). *Cyp27a1*$^{-/-}$ mice, in which only CA and its derivatives are present (*41*), were similar to *Fxr*$^{-/-}$ mice in their diminished biliary tuft cell population (fig. S3H). Together, these results suggest that CA and its metabolites negatively regulate GB and EHBD tuft cell abundance.

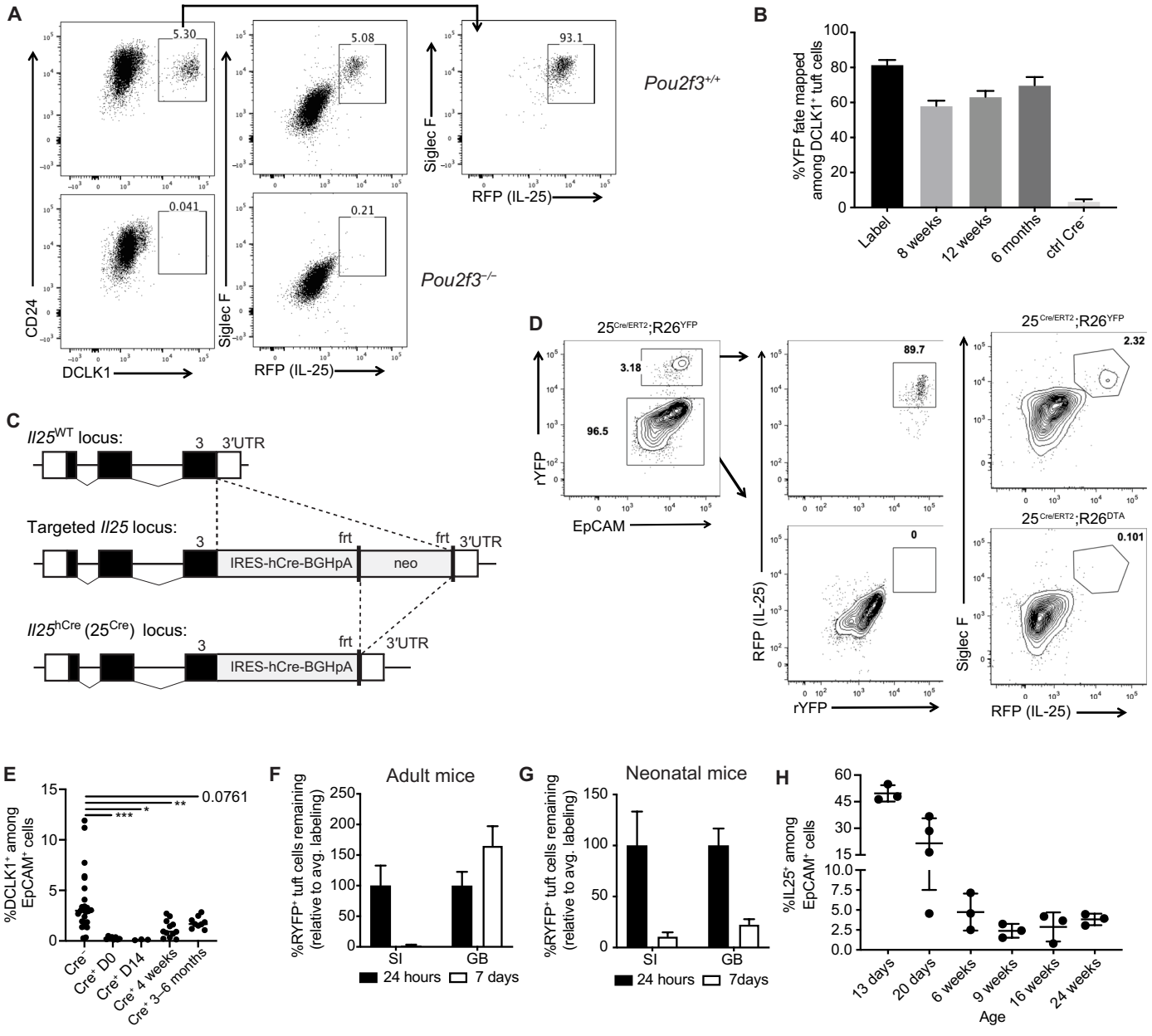

Fig. 2. Biliary tuft cells exhibit developmental regulation. (**A**) Total GB/EHBD digests from Flare25 reporter WT or *Pou2f3*$^{-/-}$ mice examined by flow cytometry for tuft cell surface markers (CD24 and Siglec F), expression of DCLK1 (intracellular staining), and endogenous RFP (IL-25). Previously gated on live singlets, FSC-A × SSC-A, EpCAM^{+}. (**B**) Dclk1$^{ERT2/+}$;R26^{YFP} mice received tamoxifen for 2 weeks. Percent YFP expression among DCLK1^{+} epithelial cells was examined in total biliary GB/EHBD digests by flow cytometry after tamoxifen removal (label) and for indicated chase periods. (**C**) Targeting strategy for IL-25 humanized Cre mice. 3′UTR, 3′ untranslated region. (**D**) Coexpression of IL-25 reporter and 25^{Cre}-driven YFP expression in 25$^{Cre/ERT2}$;R26$^{YFP/+}$ and loss of RFP^{+} tuft cells in 25$^{Cre/ERT2}$;R26$^{DTA/+}$ mice were determined by flow cytometry. Representative flow plots. (**E**) Tuft cell frequency in biliary epithelial prep from DT-injected 25$^{Cre/+}$;R26$^{iDTR/iDTR}$ mice analyzed 1 day after DT (D0) and for indicated chase periods by intracellular staining for DCLK1. Significance was determined by one-way ANOVA. *$P < 0.05$, **$P < 0.01$, and ***$P < 0.001$. (**F** and **G**) 25$^{ERT/ERT2}$;R26$^{YFP/YFP}$ adult (G) or neonatal (postnatal days 10 to 12) (**H**) mice were injected with tamoxifen; YFP expression among IL-25^{+} tuft cells was quantified in biliary epithelial prep by flow cytometry 24 hours and 7 days after the second injection. Data shown as percentage loss of YFP labeling relative to average 24 hours. YFP expression in IL-25^{+} tuft cells. (H) IL-25^{+} tuft cells in biliary epithelial prep were quantified by flow cytometry from Flare25 mice of the indicated ages.

Inflammatory cell infiltration induced by bile duct ligation increases in the absence of tuft cells

Bile duct ligation (BDL) is an established model in which altered BA levels, including increased CA (*42*, *43*), lead to cholestatic liver injury and liver fibrosis (*44*). We observed significantly reduced biliary tuft cell frequency 7 days after BDL as compared with sham surgery controls (Fig. 3, K and L).

In contrast to genetic and dietary BA manipulations, BDL induces a robust inflammatory response (Fig. 3M). Therefore, we asked whether biliary tuft cells could play a role in cholestatic biliary

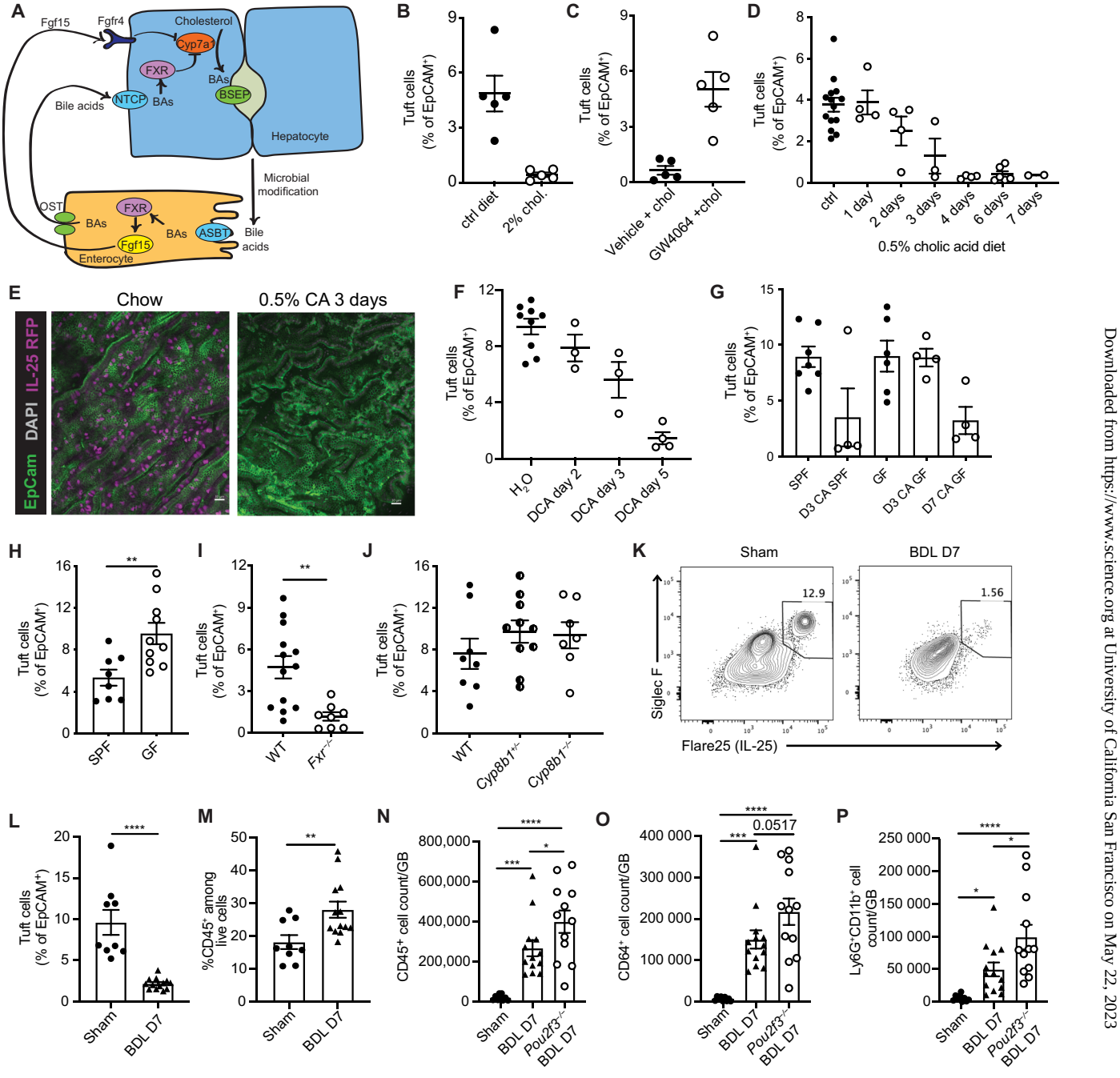

Fig. 3. Biliary tuft cell abundance is modulated by BAs. (**A**) Schematic of BA regulation via enterohepatic recirculation. (**B**) Flare25 mice were fed control (ctrl) diet or 2% cholestyramine (2% chol) diet for 2 weeks. IL-25$^+$ tuft cell frequency in biliary epithelial prep was determined by flow cytometry. Representative of three experiments. (**C**) Flare25 mice fed 2% cholestyramine diet for 10 days were injected intraperitoneally every other day with GW4064 (GW4064 + chol) or vehicle (veh + chol) starting on day 1 of diet. Representative of three experiments. (**D**) Flare25 mice were fed 0.5% CA diet for the indicated time periods. IL-25$^+$ tuft cell frequency in biliary epithelial prep was determined by flow cytometry. (**E**) Whole-mount confocal imaging of Flare25 GB from mice fed chow or 0.5% CA diet for 3 days. (**F**) GF mice were fed irradiated 0.5% CA diet in sterile isolators. Frequency of DCLK1$^+$ tuft cells among epithelial cells in total GB/EHBD digest was examined by flow cytometry at indicated time points and compared with SPF mice fed irradiated 0.5% CA diet. (**G**) Flare25 mice received 0.2% sodium deoxycholate in drinking water ad libitum. Tuft cell frequency among epithelial cells from total GB/EHBD digest was determined by flow cytometry. (**H** and **I**) Frequency of DCLK1$^+$ tuft cells among epithelial cells from total GB/EHBD digests was analyzed by flow cytometry in age- and sex-matched (H) SPF mice from the UCSF vivarium compared with GF mice and (I) *Fxr*$^{-/-}$ and WT controls. (**J**) The frequency of IL-25$^+$ tuft cells among biliary epithelial cells from total GB/EHBD digests was examined by flow cytometry in Flare25 reporter *Cyp8b1*μ, *Cyp8b1*$^{+/-}$, and *Cyp8b1*$^{+/+}$ mice. (**K** to **M**) Flare25 mice were subjected to BDL or sham surgery. Seven days later, total GB/EHBD digests were analyzed by flow cytometry for frequency of IL-25$^+$ tuft cells among epithelial cells (K and L) and frequency of CD45$^+$ immune cells (M). (**N** to **P**) Total GB/EHBD digests from *Pou2f3*$^{-/-}$ and littermate controls were analyzed by flow cytometry 7 days after BDL or sham surgery. Total immune cells (CD45$^+$) (N), macrophages (CD64$^+$CD11b$^+$Ly6G$^-$) (O), and neutrophils (Ly6G$^+$CD11b$^+$CD64$^-$) (P) were enumerated. Significance was determined by unpaired two-tailed *t* test (H, I, and M) or one-way ANOVA (N to P). **P* < 0.05, ***P* < 0.01, ****P* < 0.001, and *****P* < 0.0001.

inflammation. One week after surgery, *Pou2f3*$^{-/-}$ mice had modestly increased mortality (fig. S3I) and weight loss (fig. S3J), and we observed a trend toward increased serum bilirubin (fig. S3K) as compared with littermate controls. Neither genotype developed liver fibrosis 1 week after surgery, as assessed by quantification of liver hydroxyproline and *Col6a1* expression (fig. S3, L and M). *Pou2f3*$^{-/-}$ BDL mice had significantly more biliary-infiltrating CD45$^+$ cells (Fig. 3N), with a trend toward increased macrophages (Fig. 3O) and a significant increase in neutrophils (Fig. 3P), as compared with tuft cell–sufficient BDL mice. Extrahepatic epithelial cell hyperplasia after BDL was comparable between genotypes (fig. S3N), suggesting that increased tissue hyperplasia did not explain the increased immune cells. Hepatic ductal reaction was evident 1 week after BDL but was unaffected by loss of tuft cells (fig. S3, O and P). There was no evidence of intrahepatic IL-25$^+$ tuft cells in liver from Flare25 mice subjected to BDL (fig. S3P). Together, the loss of tuft cells was correlated with enhanced myeloid cell infiltration and a trend toward increased morbidity and mortality after BDL.

Tuft cell–deficient *Pou2f3*$^{-/-}$ mice develop spontaneous biliary neutrophil infiltration

The altered myeloid cell infiltration in *Pou2f3*$^{-/-}$ mice subjected to BDL prompted us to examine the biliary myeloid compartment in *Pou2f3*$^{-/-}$ mice at homeostasis. We found spontaneous accumulation of CD45$^+$ cells, predominantly neutrophils, in tuft cell–deficient mice compared with age- and sex-matched control mice (Fig. 4, A and B) and replicated this finding in littermate *Pou2f3*$^{-/-}$ and control mice (Fig. 4, C to E). Neutrophilia was not evident in spleen, small intestine lamina propria, or peripheral blood of *Pou2f3*$^{-/-}$ mice relative to littermate controls (fig. S4, A and B).

We next tested whether neutrophil infiltration could be induced by acute tuft cell depletion. IL-25$^+$ tuft cells were depleted in DT-treated 25$^{Cre/+}$;R26$^{iDTR/iDTR}$ mice in all tissues, but our recovery time course indicated long-term suppression of biliary tuft cells. Adult DT-injected 25$^{Cre/+}$;R26$^{iDTR/iDTR}$ mice analyzed after 4 weeks to 6 months had reduced tuft cell frequency (Fig. 4F) and increased biliary neutrophils as compared with DT-injected 25$^{+/+}$;R26$^{iDTR/iDTR}$ littermate controls (Fig. 4G and fig. S4C). Similar increases in biliary neutrophils occurred in mice subjected to DT-mediated tuft cell depletion shortly after weaning (4 weeks; Fig. 4, H and I, and fig. S4, D and E).

We next asked whether noninflammatory BA-induced tuft cell loss would promote biliary neutrophil influx. When we quantified biliary neutrophils in *Cyp27a1*$^{-/-}$ and *Fxr*$^{-/-}$ mice relative to controls, we found reduced frequency of biliary neutrophils (fig. S4, F and G). To further examine the impact of increased BA on biliary neutrophils, we fed *Pou2f3*$^{-/-}$ and littermate control mice 0.5% CA for 21 days, which, in tuft cell–sufficient mice, led to sustained tuft cell depletion (fig. S4H). Prolonged elevated dietary CA reduced immune cell infiltration in *Pou2f3*$^{-/-}$ mice, largely eliminating neutrophil influx (fig. S4I), in contrast to what we observed with tuft cell deletion under normal BA production and in cholestasis (BDL).

Loss of tuft cells drives accumulation of activated neutrophils and altered biliary epithelium

To understand how loss of biliary tuft cells affects the extrahepatic biliary immune niche, we performed scRNA-seq on total GB/EHBD

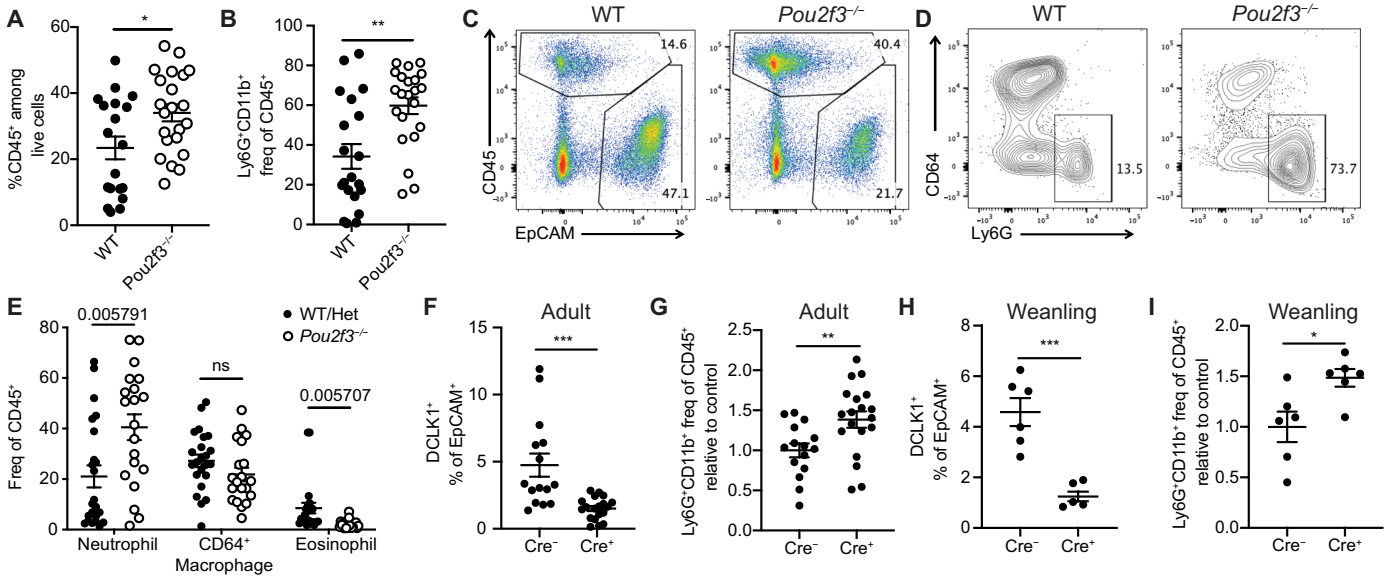

Fig. 4. *Pou2f3*$^{-/-}$ mice have increased biliary neutrophil infiltration under homeostatic conditions. (**A** and **B**) Relative frequency of CD45$^+$ cells (among live cells) (A) and neutrophils (Ly6G$^+$CD11b$^+$CD64$^-$ among CD45$^+$ cells) (B) as assessed by flow cytometry on total GB/EHBD digests from nonlittermate age- and sex-matched *Pou2f3*$^{-/-}$ and WT mice. Statistical significance was determined by unpaired two-tailed *t* test. (**C** to **E**) Total GB/EHBD digests from littermate *Pou2f3*$^{-/-}$ and control mice were analyzed by flow cytometry for the presence of CD45$^+$ cells (representative flow plot previously gated on live singlets, FSC-A × SSC-A) (C) and frequency of neutrophils (Ly6G$^+$CD11b$^+$CD64$^-$), macrophages (CD64$^+$CD11b$^+$Siglec F$^-$Ly6G$^-$), and eosinophils (Siglec F$^+$CD11b$^+$Ly6G$^-$CD64$^+$) among CD45$^+$ cells (D and E). *P* values were calculated by one-way ANOVA (E). (**F** to **I**) 25$^{Cre/+}$;Rosa^{iDTR} or 25$^{+/+}$;Rosa^{iDTR} littermate mice received two retro-orbital injections of DT. Frequency of tuft cells among epithelial cells (F and H) and neutrophils among CD45$^+$ cells (G and I) in total GB/EHBD digests were determined by flow cytometry. (F and G) Adult mice were injected at 8 weeks of age and chased 1 to 6 months. Data were pooled from four experiments. (H and I) Mice were injected at weaning and analyzed 4 to 6 weeks later. Data were pooled from two experiments. (G and I) Neutrophil frequencies were normalized to the average of control Cre mice per experiment. Statistical significance was determined by unpaired two-tailed *t* test (F to I). **P* < 0.05, ***P* < 0.01, and ****P* < 0.001. ns, not significant.

digests from *Pou2f3*$^{-/-}$ or littermate control mice (fig. S5A). We identified all major cellular types by canonical gene expression in both genotypes (Fig. 5, A and B, and fig. S5B).

As expected, neutrophils were the dominant immune population in *Pou2f3*$^{-/-}$ mice (Fig. 5C). Subclustering CD45$^+$ immune cells and assessing the cluster representation of each genotype revealed multiple neutrophil clusters, all of which were increased in *Pou2f3*$^{-/-}$ mice (Fig. 5C, fig. S5C, and table S2). Biliary neutrophils in *Pou2f3*$^{-/-}$ mice had a more activated phenotype, characterized by up-regulation of chemotaxis/cytokine response genes by GO term enrichment analysis (fig. S5D). We also observed increased expression of *Siglecf* and *Ffar2* (fig. S5E), aligning with recently described gene profiles of tissue-infiltrating neutrophils (*45*, *46*). We confirmed the higher frequency of biliary Siglec F$^+$ neutrophils in *Pou2f3*$^{-/-}$ mice as compared with littermate controls using flow cytometry (Fig. 5D and fig. S5F). We also observed a significant increase in Siglec F$^+$ neutrophils when tuft cells were depleted by DT injection in 4-week-old 25$^{Cre/+}$;R26$^{iDTR/iDTR}$ mice as compared with littermate controls (Fig. 5E).

We next analyzed the sequenced epithelial cells. Subclustering revealed highly distinct extrahepatic biliary epithelial cell gene expression programs (Fig. 5F and table S3), suggesting distinct biliary epithelial cell identities. We found major shifts in epithelial cell cluster representation in mice lacking tuft cells (Fig. 5G and fig. S5G). *Pou2f3*$^{-/-}$ mice, which lacked tuft cells as expected, had an increase in cells in cluster 2, which expressed genes such as *Cxcl5* and *Lcn2*, and loss of two epithelial clusters of unknown function: clusters 7 (*Chil4*$^+$) and 10 (*Cd247*$^+$; Fig. 5, F and G).

Previous single-cell analyses have demonstrated heterogeneous gene expression among tuft cells (*47*, *48*). Although all biliary tuft cells expressed canonical tuft cell genes including *Avil* and *Trpm5*, subclustering revealed four distinct gene expression programs (fig. S5, H to J, and table S4) that did not align with previously described "tuft-1" and "tuft-2" subsets (fig. S5, J and K).

Enrichment analysis of up-regulated genes among all *Pou2f3*$^{-/-}$ epithelial cells relative to control cells suggested increased inflammatory/defense pathways, including those related to neutrophil chemotaxis and response to bacteria (Fig. 5H). To verify this, we isolated RNA from extrahepatic biliary tissue (bile, GB, cystic, and common duct) and examined the expression of top differentially expressed genes (DEGs) up-regulated in cluster 2 epithelial cells from *Pou2f3*$^{-/-}$ mice (fig. S5L). We observed up-regulation of the genes *Cxcl5*, *Nos2*, *S100a8*, and *Il1b* in biliary tissue from *Pou2f3*$^{-/-}$ mice relative to controls (Fig. 5I).

Biliary inflammatory tone and neutrophil influx is driven by host microbiota

This inflammatory tissue signature, coupled with the enrichment in GO terms related to bacterial responses driven by the increased prevalence of cluster 2 inflammatory epithelial cells in *Pou2f3*$^{-/-}$ mice (fig. S6A), prompted us to examine whether biliary neutrophil infiltration could be affected by the microbiome. We examined the frequency of immune cells in GB/EHBDs from UCSF-housed mice as compared with mice from the Jackson Laboratory (Jax) and GF mice and found increased frequency of total CD45$^+$ immune cells and lymphocyte antigen 6 complex locus G6D (Ly6G)$^+$ neutrophils in UCSF mice compared with Jax and GF mice; neutrophils were near absent in GF mice (Fig. 6, A and B). Consistent with this, biliary tissue from Jax mice had lower expression of *Cxcl5*, *Nos2*, *S100a8*, and *Il1b* in biliary tissues from Jax mice as compared with UCSF mice (fig. S6B).

In UCSF-housed wild-type (WT) mice, we found that the reduced tuft cell frequency after weaning correlated with expansion of CD45$^+$ infiltrating immune cells (fig. S6, C and D), suggesting that the postweaning microbiome is required for biliary neutrophil influx. We observed no differences in biliary immune cell infiltration and a paucity of biliary neutrophils in both *Pou2f3*$^{-/-}$ and littermate controls analyzed at weaning (Fig. 6, C and D).

To determine whether transfer of microbiota from UCSF-housed WT mice could induce biliary neutrophil influx, we colonized Jax mice with fecal or small intestinal content from UCSF donor mice and examined biliary immune cells 6 weeks later. Mice that received microbiome transfer had higher levels of biliary infiltrating neutrophils compared with uncolonized Jax mice housed in the UCSF vivarium (Fig. 6E), whereas tuft cell frequency was unchanged (fig. S6E). We also observed an increase in the frequency of lineage-negative RORγt$^+$ lymphocytes, but not ILC2s, in colonized mice (Fig. 6F and fig. S6F). Analysis of RAR-related orphan receptor gamma t (RORγt)$^+$ lymphocytes in *Pou2f3*$^{-/-}$ and control mice suggested that this was not tuft cell dependent (fig. S6G).

This prompted us to explore the role of adaptive lymphoid cells versus ILCs in microbiome-dependent neutrophil influx. When *Rag2*$^{-/-}$ or *Rag2/Il2rg*$^{-/-}$ mice, which lack most adaptive and innate lymphocytes, were cohoused with UCSF donors, *Rag2*$^{-/-}$ recipients had robust induction of RORγt$^+$ lymphocytes; these cells were not present in *Rag2/Il2rg*$^{-/-}$ mice (Fig. 6G). Compared with uncolonized controls, cohoused *Rag2*$^{-/-}$ mice had significantly increased biliary neutrophils (Fig. 6H); the frequency of biliary neutrophils in colonized *Rag2/Il2rg*$^{-/-}$ mice was not significantly increased relative to controls (Fig. 6H).

Having established the transferability of neutrophil-promoting microbiota, we asked whether this could affect tuft cell frequency in GF mice, which have significantly more tuft cells than SPF mice. We compared GF controls with GF mice cohoused with UCSF donors or GF mice colonized with small intestinal content. Colonization with small intestinal contents from UCSF-raised donors induced biliary neutrophilia (Fig. 6I) and a reduction in biliary tuft cells (Fig. 6J) in GF mice.

DISCUSSION

Although critical to understanding human disease, immune responses in the extrahepatic biliary tree are poorly characterized. Here, we show that tuft cells, which are highly abundant in GB/EHBDs, affect the immune balance in this tissue. Biliary tuft cells express the core tuft cell gene expression program and a tissue-specific gene signature. In contrast to small intestinal tuft cells, biliary tuft cells are highly sensitive to BAs and not regulated by ILC2 cytokines. The reduction in biliary tuft cells in the BDL model of cholestasis, which superimposes inflammatory injury with elevated BA levels, correlates with increased immune cells, with the complete lack of tuft cells driving accumulation of neutrophils. Similarly, loss of tuft cells leads to spontaneous accumulation of activated neutrophils and an increase in inflammatory gene expression in unperturbed mice. Biliary neutrophil infiltration is dependent on the microbiota, which additionally affects accumulation of RORγt$^+$ lymphocytes and can promote tuft cell reduction. Our findings add to the understanding of biliary immune cells and inflammation, suggesting unappreciated mechanisms for affecting immune balance in the biliary tree that could be therapeutically targeted.

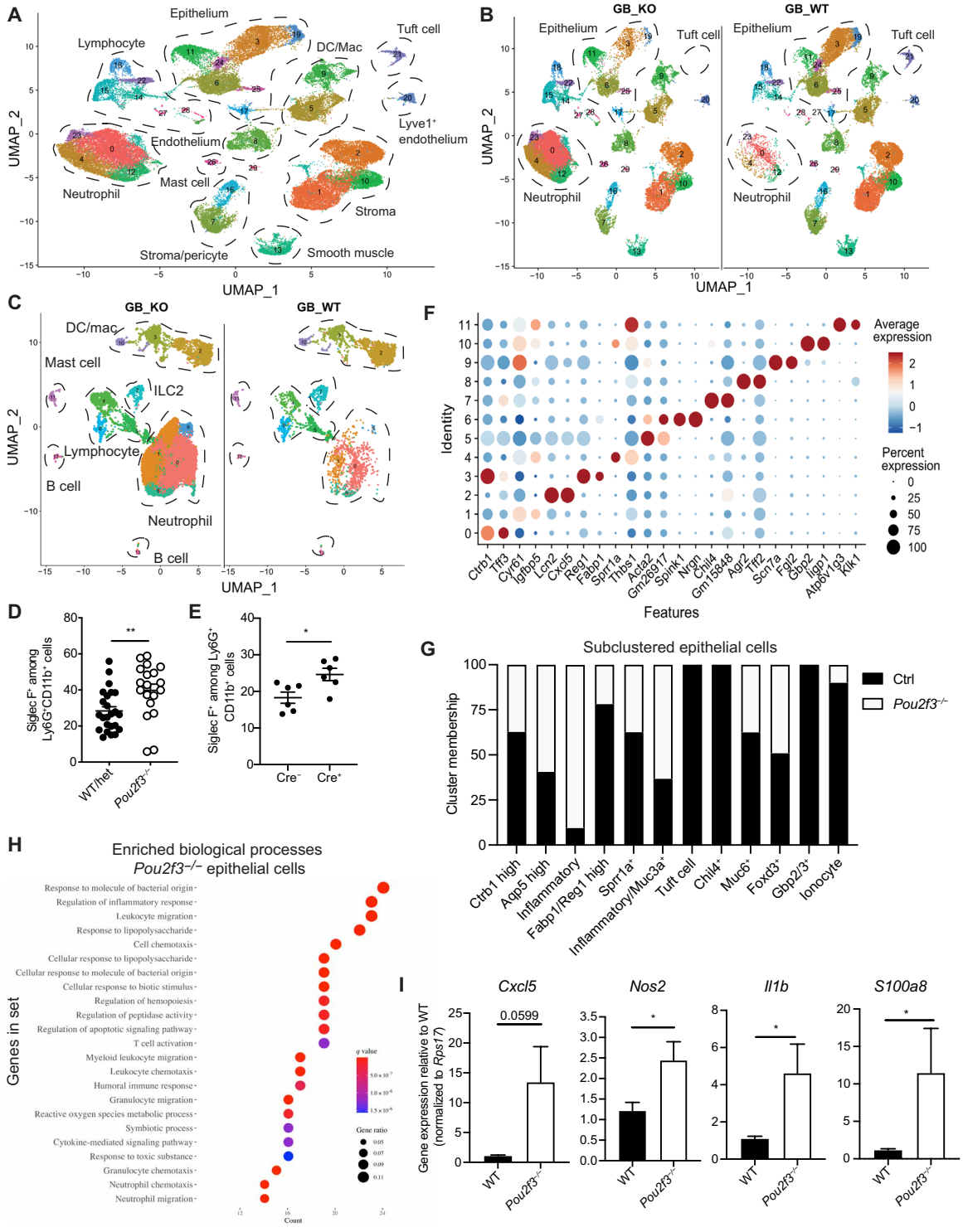

Fig. 5. Total biliary scRNA-seq reveals heightened inflammatory tone of biliary tissue in the absence of tuft cells. (**A** and **B**) Live cells were sorted from *Pou2f3*$^{-/-}$ and littermate control total GB/EHBD digests and subjected to single-cell sequencing using the 10X platform. UMAP (uniform manifold approximation and projection) shows major cell types, determined by canonical gene expression. (**C**) Subclustered CD45^{+} cells split by genotype: *Pou2f3*$^{-/-}$ (GB_KO) and littermate controls (GB_WT). (**D** and **E**) Quantification of Siglec F^{+} neutrophils from littermate *Pou2f3*$^{-/-}$ and littermate controls (D) and 25$^{Cre/+}$;R26^{iDTR} or 25$^{+/+}$;R26$^{iDTR/iDTR}$ mice injected with DT at 4 weeks of age and analyzed 4 to 6 weeks later (E) as determined by flow cytometry on total GB/EHBD digests. (**F**) Dot plot of the top two most DEGs after subclustering of biliary epithelial cells. (**G**) Epithelial cell cluster membership after normalizing to the total number of epithelial cells sequenced per genotype. (**H**) GO biological process enrichment for genes up-regulated in epithelial cells from *Pou2f3*$^{-/-}$ mice compared with controls. (**I**) Total GB/EHBD from nonlittermate *Pou2f3*$^{-/-}$ ($n = 17$) and WT ($n = 15$) mice was analyzed by qPCR for the indicated target genes relative to the housekeeping gene *Rps17*. Data were pooled from three experiments; *Pou2f3*$^{-/-}$ RQ (relative quantification) UMAP were normalized to the average of WT mice in each experiment. Statistical significance was determined by unpaired Student's *t* test. *$P < 0.05$, and **$P < 0.01$.

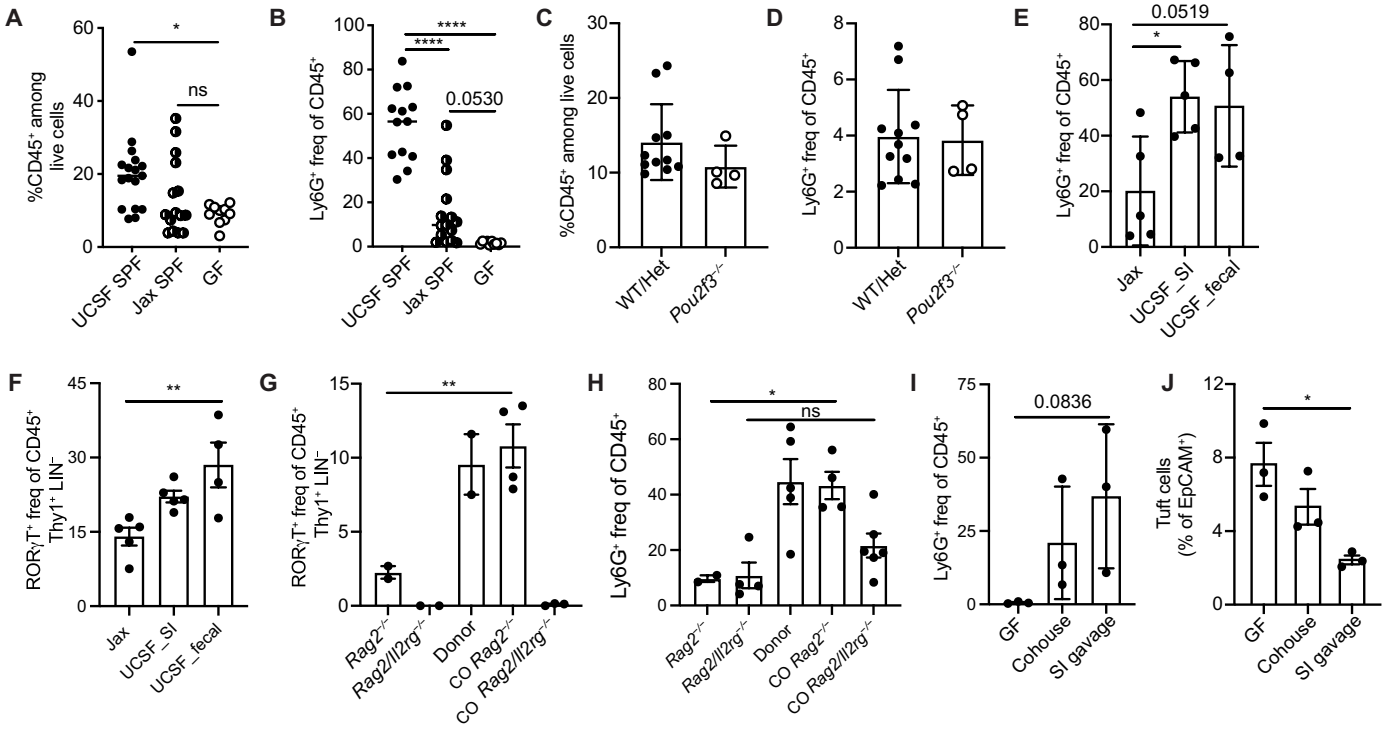

Fig. 6. Biliary neutrophilia is driven by microbiota. (**A** and **B**) Frequency CD45$^+$ cells among live cells (B) and frequency of Ly6G$^+$CD11b$^+$ neutrophils among CD45$^+$ cells (B) in total GB/EHBD digests from UCSF-housed SPF mice compared with Jax SPF mice and GF mice analyzed by flow cytometry. (**C** and **D**) Frequency CD45$^+$ cells among live cells (C) and frequency of Ly6G$^+$CD11b$^+$ neutrophils among CD45$^+$ cells (D) in total GB/EHBD digests from 3.5-week-old *Pou2f3*$^{-/-}$ mice and littermate controls analyzed by flow cytometry. (**E** and **F**) Jax mice received fecal or small intestinal contents from UCSF donor mice by oral gavage and were analyzed 6 weeks later by flow cytometry on total GB/EHBDs for frequency of Ly6G$^+$CD11b$^+$ neutrophils (E) or RORγt$^+$ lymphocytes (F) as identified by intracellular staining. (**G** and **H**) *Rag2*$^{-/-}$ or *Rag2/Il2rg*$^{-/-}$ mice from Taconic were cohoused with UCSF donor mice for 6 weeks. RORγt$^+$ lymphocytes and neutrophils were quantified by flow cytometry on total GB/EHBDs. (**I** and **J**) GF mice received small intestinal contents from UCSF donor mice by oral gavage or were cohoused with UCSF donors. Six weeks later, mice were compared with GF controls by flow cytometry on total GB/EHBDs analyzing frequency of Ly6G$^+$CD11b$^+$ neutrophils (I) or tuft cells (J) by intracellular staining. *P* values were calculated by one-way ANOVA. **P* < 0.05, ***P* < 0.01, and *****P* < 0.0001. All data shown ±SEM.

The GB/EHBDs undergo dramatic postnatal development in response to stabilization of diet, microbiome, and enterohepatic recirculation; this development is synchronous with substantial liver growth and increasing metabolic demand (*1*, *33*, *35*). Biliary tuft cells are prevalent in the preweaning period and decrease to adult levels around 6 to 8 weeks, after the period of growth and metabolic consolidation in which BA synthesis increases (*33*). Although this developmental reduction is consistent with the negative relationship between CA/CA metabolites and biliary tuft cells that we established through manipulation of enterohepatic circulation, genetic knockouts, and dietary CA, the precise mechanism driving the inverse relationship of CA and biliary tuft cell abundance remains unclear and a focus of future investigation.

Loss of tuft cells led to increased biliary infiltration of neutrophils with a transcriptomic signature similar to that seen in neutrophils in other inflammatory settings (*45*, *46*, *49*). Accumulation of inflammatory neutrophils was not observed in other tissues in *Pou2f3*$^{-/-}$ mice, suggesting a biliary-specific consequence for tuft cell loss, which could be induced by 25^{Cre}-mediated tuft cell deletion. Tuft cell loss induced by elevated levels of BAs in the absence of other inflammatory insult did not induce neutrophil influx; rather, overabundance of CA induced by dietary manipulation or genetic deficiency repressed immune cell infiltration, even in tuft cell–deficient mice. Given the robust link that we identified between microbiota and neutrophil influx, it is plausible that impacts of altered BAs on the microbiome itself could explain the disconnect between BA-induced loss of tuft cells and inducible or constitutive loss of tuft cells in driving neutrophil influx and inflammatory tissue tone.

Our single-cell and total tissue analysis suggests that loss of tuft cells promotes an antimicrobial gene expression program in the biliary epithelium [e.g., *Cxcl5* (*50*), *Lcn2* (*51*), and *S100a8/a9* (*52*)]. This tissue gene signature, and corresponding neutrophil influx, can be modulated by the microbiome. Whether the epithelium itself induces neutrophil recruitment directly (through chemotactic factors such as CXCL5) remains to be tested.

Our GB and EHBD atlas of epithelial, immune, and stromal cells extends previous efforts to analyze this tissue in mouse (*53*) and complements recent analysis of human biliary epithelium (*54*). We document extensive, previously undescribed heterogeneity of biliary epithelial and immune cells. A deeper analysis of these populations and their role in both biliary disease and normal function is clearly warranted. This sequencing was performed on "total" biliary digests (GB and ducts). Therefore, distinct epithelial cell transcriptional profiles and immune cell phenotypes could be regional. This could be the case for tuft cells themselves: The majority of tuft cells from the single-cell analysis overlap with the bulk RNA-seq data from GB tuft cells only, whereas a minority show a distinct gene expression program and could be ductal.

The inflammatory biliary tissue gene signature observed in the absence of tuft cells, coupled with infiltration of activated neutrophils, shares similarities with hallmarks of the inflamed mucosa in inflammatory bowel disease and in intestinal response to pathogenic bacteria (*55*–*58*). However, the existence of a biliary microbiome is controversial in health (*59*, *60*). Microbiome-dependent effects on the biliary tree could be regional (common duct versus GB), related to bacterial infiltration from the small intestine, or induced from microbiome-dependent metabolites or microbial by-products that could directly engage biliary tuft cells.

Understanding the complex interplay between biliary immunity, BAs, tuft cells, and the microbiome has great potential to improve understanding of biliary inflammation in health and disease. Our observations raise the intriguing possibility that biliary tuft cells may be key to limiting inflammatory responses to microbial exposures and that this may condition biliary immune tone in a way that affects progression of, or predisposition to, common biliary maladies.

MATERIALS AND METHODS

Study design

The aim of this study was to understand the phenotype/function of IL-25$^+$ tuft cells in the extrahepatic biliary tree. To this end, we optimized methods for isolation of live cells from murine GB/EHBDs; developed new genetically modified mice; and used dietary, pharmacological, genetic, and surgical perturbation of BA recirculation. We performed scRNA-seq, reverse transcription polymerase chain reaction (PCR), flow cytometry, and histology. All experiments used randomly assigned mice without investigator blinding. All data points and *n* values reflect biological replicates. Raw data are available in table S5.

Mice

Mice were housed in the University of California San Francisco SPF animal facility in accordance with Institutional Animal Care and Use Committee guidelines. Mice were ≥6 weeks old, unless otherwise noted. Experiments were performed using sex- and age-matched mice or littermate controls as indicated. *Fxr*$^{-/-}$ (Nr1h4^{tm1Gonz}/J) were purchased from the Jackson Laboratory and maintained in-house. *Rag2*$^{-/-}$ and *Rag2*$^{-/-}$*Il2rg*$^{-/-}$ mice were purchased from Taconic. *Cyp27a1*$^{-/-}$ (B6.129-Cyp27a1^{tm1Elt}/J) were provided by the Cyster Lab at UCSF. *Pou2f3*$^{-/-}$ (C57BL/6N-Pou2f3$^{tm1.1(KOMP)Vlcg}$) were provided by the Anderson Lab at UCSF (*22*). IL-25 reporter mice (Flare25), arginase-1 reporter mice (Yarg, B6.129S4-Arg1^{tm1Lky}/J), IL-5 reporter/Cre KO/KI mice [Red5, B6(C)-Il5$^{tm1.1(icre)Lky}$/J], and IL-13 [Smart13, B6.129S4(C)-Il13tm2.1Lky/J] reporter mice have been described previously (*6*, *10*, *27*, *61*). IL-5 deleter mice were generated by intercrossing Red5 mice with Rosa-DTA mice [B6.129P2-Gt(ROSA)26Sor$^{tm1(DTA)Lky}$/J] to generate homozygous RRDD mice. *IL4ra*$^{-/-}$ mice (*62*) were provided by F. Brombacher and backcrossed ≥8 generations to C57BL/6J. *Il25*$^{-/-}$ mice (*63*) were provided by A. McKenzie and backcrossed ≥8 generations to C57BL/6J. *Dclk1* CreERT2 (*32*) from M. Buchert at the Olivia Newton John Cancer Research Institute, Australia were intercrossed with YFP Gt(ROSA)26STOP-flox, provided by O. Klein at UCSF.

Generation of new mouse strains

Il25-driven Cre and CreERT2

The 25^{Cre} and 25^{ERT} mice were generated as described for the IL-25 reporter allele Flare25 (*10*), with the following modifications: (i) The 5′ loxP (locus of x-over, P1) site in front of the last exon of *Il25* was removed from the 5′ homologous arm, and (ii) a humanized (eukaryotic codon-optimized) Cre (for 25^{Cre}) or tandem red fluorescent protein (RFP) and tamoxifen-inducible Cre recombinase (for 25^{ERT2}) (*64*) was used to replace the tandem RFP fluorescent protein sequence in the original Flare25.

Cyp8b1$^{-/-}$ *mice*

Two single guide RNAs (sgRNAs) targeting the *Cyp8b1* gene main exon (GGCATCCCACAACCGTGAGC and GATCCGTCGCGGAGATAAGG) and recombinant Cas9 (PNA Bio) were simultaneously injected as ribonucleoproteins into the zygotes of C57BL/6J homozygous reporter mice (Flare25, Yarg, Smart13; Gladstone Institutes, San Francisco, CA). Founders were screened by PCR using primers AGCCTGCTGGAGCCTAGCCATGACG and AGCTGGGGAGAGGAAGGAGTGCCTC to identify the 1.2-kb deletion event that resulted from the end-joining event of two double-stranded breaks at the sgRNA-targeted sites. Individual positive founder was backcrossed with WT homozygous reporter mice to segregate the alleles before intercrossing to obtain homozygous *Cyp8b1* knockouts.

GF mice

GF mice were from the UCSF Gnotobiotic Core Facility. Feeding experiments were performed in gnotobiotic isolators. Fecal pellet DNA was examined by quantitative PCR (qPCR) to verify the absence of bacterial colonization.

Preparation of single-cell suspensions

GB, cystic duct, and common duct (at the duodenum) were resected. Hepatocytes/pancreas were removed by scraping. GB was fileted, and tissue was rinsed in cold Hanks' balanced salt solution (HBSS; Ca^{2+}/Mg^{2+}-free; Life Technologies). Tissue was incubated at 37°C for 10 min in 1 ml of HBSS (Ca^{2+}/Mg^{2+}-free) with 2% fetal calf serum (FCS; Atlanta Biologicals), 10 mM Hepes (Sigma-Aldrich), and 5 mM dithiothreitol (Sigma-Aldrich). Supernatants were discarded, and tissue was incubated at 37°C for 20 min in 1 ml of HBSS (Ca^{2+}/Mg^{2+}-free) with 2% FCS and 5 mM EDTA (Teknova). Supernatant was collected into fluorescence-activated cell sorting wash buffer [FWB; phosphate-buffered saline (PBS), 3% FCS, and 0.05% NaN_3] and kept on ice. This step was repeated. After the collection of the EDTA supernatant, cells were pelleted and resuspended in FWB. For epithelial prep, cells were then stained for flow cytometry. For total GB/EHBD, the remaining tissue was incubated at 37°C for 5 min in 1 ml of HBSS (with Ca^{2+}/Mg^{2+}) with 3% FCS and 10 mM Hepes; the supernatant was discarded; and the tissue was minced and digested at 37°C for 20 to 25 min in 4 ml of HBSS (with Ca^{2+}/Mg^{2+}) supplemented with 3% FCS, 10 mM Hepes, Liberase (100 μg/ml; Roche), and deoxyribonuclease I (30 μg/ml; Roche). Incubations were performed with gentle rocking. Tissue was dissociated in GentleMACS C tubes (Miltenyi Biotec) using program m_intestine_01. The epithelial fraction in cold FWB was digested, passed through a 100-μm filter, and washed in cold FWB. Small intestine epithelium and lamina propria were processed as described (*15*, *65*).

In vivo manipulations

CA [0.5% (w/w)] in Teklad 7001 or Teklad 2019 base diet was from Envigo. Cholestyramine [2% (w/w); Sigma-Aldrich] diet on AIN93G was made by Research Diets. Sodium DCA [0.2% (w/v); Sigma-Aldrich] was dissolved in sterile water. Tamoxifen (Sigma) treatment was performed by intraperitoneal injection or given in chow (Envigo, TD.130858) (*64*), as indicated in legends. Tamoxifen was dissolved

in ethanol/Cremophor at 20 mg/ml and diluted 1:1 in sterile PBS, and mice received 1 mg in 100 µl. Tamoxifen chow was provided for 2 to 4 weeks. Labeling was assessed 24 hours after the last injection/removal of diet. DT (Sigma) was injected retro-orbitally (500 ng/100 µl of sterile PBS per mouse). Two injections were given 48 hours apart, and mice were analyzed for deletion after 24 hours. GW4064 (SelleckChem) was dissolved in dimethyl sulfoxide, resuspended in sterile methylcellulose, and given intraperitoneally at 100 mg/kg body weight.

Microbiota transfer

GF/Jax mice were cohoused for a minimum of 6 weeks with adult UCSF-raised WT females with known biliary neutrophil infiltration. For microbiota transfer, the full length of the small intestine from affected UCSF-housed WT donor mice was fileted and flushed with sterile PBS, followed by gentle scraping with curved forceps (into a total volume of 5 to 7 ml), or fecal pellets were homogenized in PBS (two donors; volume, 5 ml). Slurry was filtered through a 100-µm filter. Recipient mice received 150 µl by oral gavage.

BA quantification

Mice were fasted overnight with access to water. After euthanasia, GB/EHBDs were resected as described above; intact GB (containing bile) was snap-frozen in liquid nitrogen and stored at −80°C. Taurocholic acid and taurodeoxycholic acid were quantified by gas chromatography–mass spectrometry (West Coast Metabolomics, University of California, Davis).

Total tissue RNA extraction and qPCR

GBs with bile, cystic, and common duct or liver were snap-frozen in liquid nitrogen or on dry ice and stored at −80°C. Samples were dissociated in 1 ml of RNAzol (Molecular Research Center, Inc.) using Miltenyi M tubes and the gentleMACS tissue dissociator (Miltenyi Biotec) RNA1 program. RNA was isolated following the manufacturer's protocol with additional BAN phase separation. RNA was subjected to reverse transcription using the SuperScript VILO Master Mix (Life Technologies). cDNA was used as template for qPCR with the Power SYBR Green reagent on a StepOnePlus cycler (Applied Biosystems). Transcripts were normalized to *Rps17* (40*S* ribosomal protein S17) expression and relative expression shown as 2-ΔΔCt compared with the average ΔCt of experiment-matched controls using the following primers: *Rps17*, 5′-CGCCATTATCCCCAGCAAG-3′ and 5′-TGTCGGGATCCACCTCAATG-3′; *Fgf15*, 5′-GAGGACCAAAACGAACGAAATT-3′ and 5′-ACG TCC TTG ATG GCA ATCG-3′; *Cyp7a1*, 5′-GGGATTGCTGTGGTAGTGAGC-3′ and 5′-GGTATGGAATCAACCCGTTGTC-3′ (PrimerBank, 31542445a1); *Nos2*, 5′-GAATCTTGGAGCGAGTTGTGG-3′ and 5′-CAGGAAGTAGGTGAGGGCTTG-3′; *Il1b*, 5′-GCAACTGTTCCTGAACTCAACT-3′ and 5′-ATCTTTTGGGGTCCGTCAACT-3′; *S100a8*, 5′-AAATCACCATGCCCTCTACAAG-3′ and 5′-CCCACTTTTATCACCATCGCAA-3′ (PrimerBank, 7305453a1); *Col1a1*, 5′-CCAAGAAGACATCCCTGAAGTCA-3′ and 5′-TGCACGTCATCGCACACA-3′; *Epcam*, 5′-GCGGCTCAGAGAGACTGT-3′, 5′-CCAAGCATTTAGACGCCAGTTT-3′; *Cxcl5*, 5′-TCCAGCTCGCCATTCATGC-3′ and 5′-TTGCGGCTATGACTGAGGAAG-3′ (PrimerBank, 6677887a1); and *Cyp8b1*, 5′-TGTTTCTGGGTCCTCTTATTCCTGC-3′ and 5′-ACTCTCCTCCATCACGCTGTCCAAC-3′.

Bile duct ligation

Mice were anesthetized in an aseptic surgical field by intraperitoneal ketamine/xylazine (ketamine, 80 to 100 mg/kg, and xylazine, 5 to 10 mg/kg) followed by inhaled isoflurane and subcutaneous buprenorphine analgesia (0.05 to 0.1 mg/kg). The abdomen was opened by midline laparotomy about 2 cm in length, and the peritoneum was cut open along the linea alba. The operation area was spread using a Colibri retractor in the peritoneal cavity and lifted with a saline-moisturized cotton swab to reveal the hilum. The bile duct was exposed and separated from the portal vein and hepatic artery using microserration forceps. Suture (7-0) was placed around the bile duct and secured with two surgical knots. A second cranial ligation was added in the same manner. Abdominal layers (peritoneum and cutis plus facia) were closed with running 6-0 sutures with absorbable suture material. Mice were weighed daily and monitored for reaching humane end points for euthanasia.

Whole-mount imaging

GB/EHBDs were resected, fileted to drain bile, and rinsed in cold PBS before fixation in 4% paraformaldehyde (PFA; Thermo Scientific, catalog no. 28906) for 4 hours at room temperature (RT) or overnight at 4°C. Tissue was rinsed in PBS three times, blocked with 5% serum (secondary antibody host species) in 0.1% Triton-X PBS for 1 hour, stained with primary unconjugated antibody for 2 to 4 hours at RT or overnight at 4°C, washed three times, and stained with secondary antibody and conjugated primary antibody for 1 to 2 hours at RT. Samples were washed three times and incubated in DAPI (4′,6-diamidino-2-phenylindole)/PBS 1:1000 for 10 min. Samples were washed four times and mounted on glass slides with glass coverslips in VECTASHIELD (Vector Labs). Amplification of Flare25 RFP was not necessary. Samples were scanned using a NikonA1R laser scanning confocal (405, 488, 561, and 650 laser lines) with ×20 air objective. High-resolution images were acquired in Galvano mode with pixel sizes of 300 nm. Bitplane Imaris v9.5 software package (Andor Technology PLC, Belfast, Northern Ireland) was used for image analysis.

Thick section liver staining

Animals were perfused with PBS. Liver/GB was harvested and fixed in 4% PFA overnight at 4°C. Fixed tissues were washed with PBS; cut into 200-µm sections using a vibratome (Leica VT1000S); permeabilized with 0.2% Triton X-100/0.3 M glycine in PBS for 3 to 4 hours at RT; and blocked with 0.3% Triton X-100, 5% fetal bovine serum (FBS), 0.5% bovine serum albumin (BSA), and 5% serum (host species of the secondary antibody) in PBS overnight at 4°C. Samples were incubated with primary antibodies in 0.15% Triton X-100, 7.5% FBS, 0.75% BSA, and 3% serum in PBS at 4°C overnight; washed in 0.2% Triton X-100 in PBS for 30 min three to four times; and then incubated with secondary antibodies diluted in 0.15% Triton X-100, 7.5% FBS, 0.75% BSA, and 3% serum in PBS at 4°C overnight. Samples were washed in 0.2% Triton X-100 in PBS for 30 min three to four times, followed by dehydration in ethanol gradation (20, 30, 50, 70, 95, and 100%) for 5 min each. Samples were cleared by soaking in methyl salicylate for at least 10 min. Samples were scanned using NikonA1R laser scanning confocal (405, 488, 561, and 650 laser lines) and ×16/0.8 water immersion objective. Acquisition and analysis were performed as described above. For localization of IL-5$^+$ lymphocytes in the liver and GB, a channel was generated and surfaced.

Imaging antibodies

Primary antibodies included Living Colors Rabbit Anti-DsRed Polyclonal Pan Antibody (1:200; Takara), Goat Anti-Type 1 Collagen Polyclonal Antibody (1:200; Southern Biotech), Rat Anti-CD326/EpCAM Monoclonal Antibody (1:200; clone G8.8; BD Pharmingen),

and Rabbit Anti-DCAMKL1 Monoclonal Antibody (1:300; clone EPR6085; Abcam). The following species-specific secondary antibodies were used at 1:300 dilution: Alexa Fluor 488 donkey anti-goat immunoglobulin G (IgG) (H+L) cross-adsorbed (Thermo Fisher Scientific), Alexa Fluor 488 donkey anti-rat IgG (H+L) cross-adsorbed (Thermo Fisher Scientific), Alexa Fluor 555 donkey anti-rabbit IgG (H+L) cross-adsorbed (Thermo Fisher Scientific), Alexa Fluor 647 donkey anti-goat IgG (H+L) cross-adsorbed (Thermo Fisher Scientific), and Alexa Fluor 647 donkey anti-rabbit IgG (H+L) cross-adsorbed (Thermo Fisher Scientific). The directly conjugated eFluor 660 anti-Lyve1 (lymphatic vessel endothelial hyaluronan receptor 1) monoclonal antibody (clone ALY7, eBioscience) was used at 1:200 dilution. The directly conjugated AF488 anti-CD326/EpCAM monoclonal antibody (clone G8.8, BioLegend) was used at 1:200 dilution.

Flow cytometry

Single-cell suspensions were incubated with Fc Block (Bio X Cell, 2.4G2) and stained with antibodies to surface markers diluted in FWB. Cells were washed in FWB and resuspended in FWB containing DAPI (Roche) and flow cytometric counting beads (CountBright Absolute; Life Technologies) for live cell gating and counts. Cells for intracellular staining were washed in PBS and stained with Violet Live/Dead fixable stain (Life Technologies) according to the manufacturer's instructions. Transcription factor staining was done using the FoxP3/Transcription Factor Staining Buffer Set (eBioscience) according to the manufacturer's instructions. Cells for DCLK1 staining were fixed in 4% PFA for 2 to 5 min, washed in FWB, and stained with rabbit anti-DCLK1 (1:4000; Abcam, ab31704) antibody in perm/wash buffer from the FoxP3 staining buffer kit, followed by $F(ab')_2$ donkey anti-rabbit IgG-PE (1:1000; Life Technologies) or goat anti-rabbit AF488 (1:4000; Invitrogen) for 10 min. Staining was done on ice. For costaining of DCLK1 and endogenous IL-25 RFP, PFA fixation was performed for 30 s on ice. Samples were analyzed on an LSRFortessa (BD Biosciences) with five lasers (355, 405, 488, 561, and 640 nm). Samples were FSC-A/SSC-A (forward scatter-area/side scatter-area) gated to exclude debris, FSC-H (height)/FSC-A gated to select single cells, and gated to exclude dead cells. Data were analyzed with FlowJo 9/10 (Tree Star/FlowJo).

Flow cytometry antibodies

The following flow cytometry antibodies were purchased from BioLegend: EpCAM PerCpCy5.5 and BV711 (clone G8.8), Ly6G APCCy7 (1A8), CD11b BV711 (M1/70), CD45 BV785 (30-F11), Thy-1 BV786 (30-H12), TCRγδ PerCPCy5.5 (GL3), NK1.1 PECy7 (PK136), and NKp46/CD335 PECy7 (29A1.4). Lineage-positive cells were excluded in ILC staining using the antibodies in Pacific Blue from BioLegend: CD11c (N418), F4/80 (BM8), CD11b (M1/70), FCεR1 (MAR-1), CD19 (6D5), B220 (RA3-6B2), Ter-119, and Gr-1. T1/ST2 FITC/PE (DJ8) was purchased from MD Bioproducts. The following antibodies were from eBioscience/Invitrogen: GATA3 ef660 (TWAJ) and TCRβ APC-ef780 (H57-597). The following antibodies were purchased from BD: CD64a/b AF647 (X54-5/7.1), RORγt PE (B2D), CD45 BUV395 (30-F11), Siglec-F BB515 (E50-2440), and Thy-1 BUV395 (3-H12).

RNA-seq analysis

Tuft (live, RFP^+ $EpCAM^+$) and nontuft (live, RFP^- $EpCAM^+$) cells from single-cell suspensions of GB and duodenal epithelium were sorted from three Flare25 mice into Dynabeads mRNA Direct Micro Purification kit lysis buffer (Thermo Fisher Scientific); mRNA was isolated according to the manufacturer's protocol. Amplified cDNA was prepared using the NuGEN Ovation RNA-Seq system V2 kit according to the manufacturer's protocol (NuGEN Technologies). Sequencing libraries were generated using the Nextera XT library preparation kit with multiplexing primers according to the manufacturer's protocol (Illumina). Library fragment size distributions were assessed using the Bioanalyzer 2100 and the DNA high-sensitivity chip (Agilent Technologies). Library sequence quality was assessed by sequencing single-end 50–base pair reads using the Illumina MiSeq platform and pooled for high-throughput sequencing on the Illumina HiSeq 4000 by using equal numbers of uniquely mapped reads (Illumina). Twelve samples per lane were multiplexed. Sequencing yielded a median read depth of 89.2 million reads per sample. The analytic pipeline included demultiplexing raw sequencing results, trimming adapter sequences, and aligning to the reference genome. Sequence alignment and splice junction estimation was performed using STAR software (2.7.2b). For differential expression testing, the genomic alignments were restricted to unique Ensembl IDs (all protein coding mRNAs, coding, and noncoding RNAs). STAR aggregated mappings on a per-gene basis were used as raw input for normalization by DESeq2. Differential expression analysis was performed in the R version 36.1 using DESeq2 version 1.26. Significance thresholds were false discovery rate (FDR) < 0.05 and log fold change >1 or <−1. Unsupervised PCA was performed on the top 500 genes by variance.

Shared tuft cell genes were defined as genes in SI/GB tuft cells >2 $\log_2$FC relative to nontuft cells from the same tissue, with an FDR < 0.01, and a sum normalized read count >500 in SI or GB tuft cells (413 total genes). GB tuft cell exclusive gene signature was defined as genes with FDR < 0.05 relative to SI tuft cells and GB nontuft cells. Genes were further filtered to include those with a sum normalized read count >150 in GB tuft cells (555). GO term and pathway analysis was performed using the ClusterProfiler package in R (*66*). Raw files are available in GEO with accession number GSE194035.

Single-cell sequencing

GB/EHBDs from five mice per genotype were prepared using the total digest described above. Single-cell suspensions were stained with DAPI, and live cells (DAPI negative, FSC-A × SSC-A) were sorted using a MoFlo XDP (Beckman Coulter). Concentration was determined using CountBright beads on an LSRFortessa. Single-cell libraries from 37,000 cells per sample were prepared with the Chromium Single Cell 3′ GEM, Library & Gel Bead Kit v3 (10x Genomics, PN-1000075) following the manufacturer's protocol. The libraries were sequenced on the NovaSeq 6000 at the UCSF Institute for Human Genetics with the following number of cycles for each read: read 1, 28; I7 index, 8; I5 index, 0; read 2, 91.

Data were analyzed in Seurat V3 using SCTransform normalization: min.cells = 3; min.features = 200; nFeature_RNA ≥ 300; nFeature_RNA < 5000; nCount_RNA < 20,000; percent mitochondrial reads < 15; and percent hemoglobin reads, 0.1. Percent mitochondrial reads was regressed out of clustering/aggregation. After clustering of all cells at resolution 0.6, epithelial or immune clusters were identified by canonical markers and subclustered at resolution 0.3. Contaminating doublets were removed, and the populations were clustered again before DEG analysis for cluster-defining genes and differential expression between genotypes. Tuft cells were subclustered at resolution

0.3 and were only found in cells isolated from control mice. GO term/pathway analysis was performed using the ClusterProfiler package in R (*66*).

Statistical analysis

Statistical analysis was performed using Prism 6/8 (GraphPad Software). Figures display means ± SEM. *P* values were calculated using unpaired two-tailed Student's *t* test for comparison between two groups or one-way analysis of variance (ANOVA) for multiple comparisons. Intragroup variation was not assessed. Transcriptomic data were analyzed and visualized in R, using the DESeq2 and Seurat packages for calculation of differential gene expression as described above.

SUPPLEMENTARY MATERIALS

www.science.org/doi/10.1126/sciimmunol.abj1080
Figs. S1 to S6
Tables S1 to S5

View/request a protocol for this paper from *Bio-protocol*.

REFERENCES AND NOTES

1. A. Wahlstrom, S. I. Sayin, H. U. Marschall, F. Backhed, Intestinal crosstalk between bile acids and microbiota and its impact on host metabolism. *Cell Metab.* **24**, 41–50 (2016).
2. F. W. Gorham, A. C. Ivy, *General Function of the Gall Bladder from the Evolutionary Standpoint* (American Journal of Digestive Diseases and Nutrition, 1938), vol. 22.
3. H. Higashiyama, M. Uemura, H. Igarashi, M. Kurohmaru, M. Kanai-Azuma, Y. Kanai, Anatomy and development of the extrahepatic biliary system in mouse and rat: A perspective on the evolutionary loss of the gallbladder. *J. Anat.* **232**, 134–145 (2018).
4. W. Jia, G. Xie, W. Jia, Bile acid-microbiota crosstalk in gastrointestinal inflammation and carcinogenesis. *Nat. Rev. Gastroenterol. Hepatol.* **15**, 111–128 (2018).
5. P. L. Jansen, A. Ghallab, N. Vartak, R. Reif, F. G. Schaap, J. Hampe, J. G. Hengstler, The ascending pathophysiology of cholestatic liver disease. *Hepatology* **65**, 722–738 (2017).
6. J. C. Nussbaum, S. J. Van Dyken, J. von Moltke, L. E. Cheng, A. Mohapatra, A. B. Molofsky, E. E. Thornton, M. F. Krummel, A. Chawla, H. E. Liang, R. M. Locksley, Type 2 innate lymphoid cells control eosinophil homeostasis. *Nature* **502**, 245–248 (2013).
7. L. Fabris, C. Spirli, M. Cadamuro, R. Fiorotto, M. Strazzabosco, Emerging concepts in biliary repair and fibrosis. *Am. J. Physiol. Gastrointest. Liver Physiol.* **313**, G102–g116 (2017).
8. C. E. O'Leary, C. Schneider, R. M. Locksley, Tuft cells-systemically dispersed sensory epithelia integrating immune and neural circuitry. *Annu. Rev. Immunol.* **37**, 47–72 (2019).
9. B. Schutz, I. Jurastow, S. Bader, C. Ringer, J. von Engelhardt, V. Chubanov, T. Gudermann, M. Diener, W. Kummer, G. Krasteva-Christ, E. Weihe, Chemical coding and chemosensory properties of cholinergic brush cells in the mouse gastrointestinal and biliary tract. *Front. Physiol.* **6**, 87 (2015).
10. J. von Moltke, M. Ji, H. E. Liang, R. M. Locksley, Tuft-cell-derived IL-25 regulates an intestinal ILC2-epithelial response circuit. *Nature* **529**, 221–225 (2016).
11. L. Luciano, E. Reale, Presence of brush cells in the mouse gallbladder. *Microsc. Res. Tech.* **38**, 598–608 (1997).
12. L. Luciano, M. Castellucci, E. Reale, The brush cells of the common bile duct of the rat. This section, freeze-fracture and scanning electron microscopy. *Cell Tissue Res.* **218**, 403–420 (1981).
13. T. J. Nevalainen, Ultrastructural characteristics of tuft cells in mouse gallbladder epithelium. *Acta Anat.* **98**, 210–220 (1977).
14. B. Schutz, A. L. Ruppert, O. Strobel, M. Lazarus, Y. Urade, M. W. Buchler, E. Weihe, Distribution pattern and molecular signature of cholinergic tuft cells in human gastro-intestinal and pancreatic-biliary tract. *Sci. Rep.* **9**, 17466 (2019).
15. C. Schneider, C. E. O'Leary, J. von Moltke, H. E. Liang, Q. Y. Ang, P. J. Turnbaugh, S. Radhakrishnan, M. Pellizzon, A. Ma, R. M. Locksley, A metabolite-triggered tuft cell-ILC2 circuit drives small intestinal remodeling. *Cell* **174**, 271–284.e14 (2018).
16. M. S. Nadjsombati, J. W. McGinty, M. R. Lyons-Cohen, J. B. Jaffe, L. DiPeso, C. Schneider, C. N. Miller, J. L. Pollack, G. A. Nagana Gowda, M. F. Fontana, D. J. Erle, M. S. Anderson, R. M. Locksley, D. Raftery, J. von Moltke, Detection of succinate by intestinal tuft cells triggers a type 2 innate immune circuit. *Immunity* **49**, 33–41.e37 (2018).
17. F. Gerbe, E. Sidot, D. J. Smyth, M. Ohmoto, I. Matsumoto, V. Dardalhon, P. Cesses, L. Garnier, M. Pouzolles, B. Brulin, M. Bruschi, Y. Harcus, V. S. Zimmermann, N. Taylor, R. M. Maizels, P. Jay, Intestinal epithelial tuft cells initiate type 2 mucosal immunity to helminth parasites. *Nature* **529**, 226–230 (2016).
18. M. R. Howitt, S. Lavoie, M. Michaud, A. M. Blum, S. V. Tran, J. V. Weinstock, C. A. Gallini, K. Redding, R. F. Margolskee, L. C. Osborne, D. Artis, W. S. Garrett, Tuft cells, taste-chemosensory cells, orchestrate parasite type 2 immunity in the gut. *Science* **351**, 1329–1333 (2016).
19. S. Ualiyeva, N. Hallen, Y. Kanaoka, C. Ledderose, I. Matsumoto, W. G. Junger, N. A. Barrett, L. G. Bankova, Airway brush cells generate cysteinyl leukotrienes through the ATP sensor P2Y2. *Sci. Immunol.* **5**, eaax7224 (2020).
20. A. Perniss, S. Liu, B. Boonen, M. Keshavarz, A. L. Ruppert, T. Timm, U. Pfeil, A. Soultanova, S. Kusumakshi, L. Delventhal, Ö. Aydin, M. Pyrski, K. Deckmann, T. Hain, N. Schmidt, C. Ewers, A. Günther, G. Lochnit, V. Chubanov, T. Gudermann, J. Oberwinkler, J. Klein, K. Mikoshiba, T. Leinders-Zufall, S. Offermanns, B. Schütz, U. Boehm, F. Zufall, B. Bufe, W. Kummer, Chemosensory cell-derived acetylcholine drives tracheal mucociliary clearance in response to virulence-associated formyl peptides. *Immunity* **52**, 683–699.e11 (2020).
21. L. G. Bankova, D. F. Dwyer, E. Yoshimoto, S. Ualiyeva, J. W. McGinty, H. Raff, J. von Moltke, Y. Kanaoka, K. Frank Austen, N. A. Barrett, The cysteinyl leukotriene 3 receptor regulates expansion of IL-25-producing airway brush cells leading to type 2 inflammation. *Sci. Immunol.* **3**, eaat9453 (2018).
22. C. N. Miller, I. Proekt, J. von Moltke, K. L. Wells, A. R. Rajpurkar, H. Wang, K. Rattay, I. S. Khan, T. C. Metzger, J. L. Pollack, A. C. Fries, W. W. Lwin, E. J. Wigton, A. V. Parent, B. Kyewski, D. J. Erle, K. A. Hogquist, L. M. Steinmetz, R. M. Locksley, M. S. Anderson, Thymic tuft cells promote an IL-4-enriched medulla and shape thymocyte development. *Nature* **559**, 627–631 (2018).
23. C. Bornstein, S. Nevo, A. Giladi, N. Kadouri, M. Pouzolles, F. Gerbe, E. David, A. Machado, A. Chuprin, B. Toth, O. Goldberg, S. Itzkovitz, N. Taylor, P. Jay, V. S. Zimmermann, J. Abramson, I. Amit, Single-cell mapping of the thymic stroma identifies IL-25-producing tuft epithelial cells. *Nature* **559**, 622–626 (2018).
24. B. Lucas, A. J. White, E. J. Cosway, S. M. Parnell, K. D. James, N. D. Jones, I. Ohigashi, Y. Takahama, W. E. Jenkinson, G. Anderson, Diversity in medullary thymic epithelial cells controls the activity and availability of iNKT cells. *Nat. Commun.* **11**, 2198 (2020).
25. R. R. Ricardo-Gonzalez, S. J. Van Dyken, C. Schneider, J. Lee, J. C. Nussbaum, H. E. Liang, D. Vaka, W. L. Eckalbar, A. B. Molofsky, D. J. Erle, R. M. Locksley, Tissue signals imprint ILC2 identity with anticipatory function. *Nat. Immunol.* **19**, 1093–1099 (2018).
26. J. W. McGinty, H. A. Ting, T. E. Billipp, M. S. Nadjsombati, D. M. Khan, N. A. Barrett, H. E. Liang, I. Matsumoto, J. von Moltke, Tuft-cell-derived leukotrienes drive rapid anti-helminth immunity in the small intestine but are dispensable for anti-protist immunity. *Immunity* **52**, 528–541.e7 (2020).
27. T. A. Reese, H. E. Liang, A. M. Tager, A. D. Luster, N. Van Rooijen, D. Voehringer, R. M. Locksley, Chitin induces accumulation in tissue of innate immune cells associated with allergy. *Nature* **447**, 92–96 (2007).
28. M. W. Dahlgren, S. W. Jones, K. M. Cautivo, A. Dubinin, J. F. Ortiz-Carpena, S. Farhat, K. S. Yu, K. Lee, C. Wang, A. V. Molofsky, A. D. Tward, M. F. Krummel, T. Peng, A. B. Molofsky, Adventitial stromal cells define group 2 innate lymphoid cell tissue niches. *Immunity* **50**, 707–722.e6 (2019).
29. J. Yamashita, M. Ohmoto, T. Yamaguchi, I. Matsumoto, J. Hirota, Skn-1a/Pou2f3 functions as a master regulator to generate Trpm5-expressing chemosensory cells in mice. *PLOS ONE* **12**, e0189340 (2017).
30. D. Alvaro, M. G. Mancino, S. Glaser, E. Gaudio, M. Marzioni, H. Francis, G. Alpini, Proliferating cholangiocytes: A neuroendocrine compartment in the diseased liver. *Gastroenterology* **132**, 415–431 (2007).
31. J. Lamote, G. Willems, DNA synthesis, cell proliferation index in normal and abnormal gallbladder epithelium. *Microsc. Res. Tech.* **38**, 609–615 (1997).
32. C. B. Westphalen, S. Asfaha, Y. Hayakawa, Y. Takemoto, D. J. Lukin, A. H. Nuber, A. Brandtner, W. Setlik, H. Remotti, A. Muley, X. Chen, R. May, C. W. Houchen, J. G. Fox, M. D. Gershon, M. Quante, T. C. Wang, Long-lived intestinal tuft cells serve as colon cancer-initiating cells. *J. Clin. Invest.* **124**, 1283–1295 (2014).
33. J. Y. Cui, L. M. Aleksunes, Y. Tanaka, Z. D. Fu, Y. Guo, G. L. Guo, H. Lu, X. B. Zhong, C. D. Klaassen, Bile acids via FXR initiate the expression of major transporters involved in the enterohepatic circulation of bile acids in newborn mice. *Am. J. Physiol. Gastrointest. Liver Physiol.* **302**, G979–G996 (2012).
34. G. Khandekar, J. Llewellyn, A. Kriegermeier, O. Waisbourd-Zinman, N. Johnson, Y. Du, R. Giwa, X. Liu, T. Kisseleva, P. A. Russo, N. D. Theise, R. G. Wells, Coordinated development of the mouse extrahepatic bile duct: Implications for neonatal susceptibility to biliary injury. *J. Hepatol.* **72**, 135–145 (2020).
35. N. van Best, U. Rolle-Kampczyk, F. G. Schaap, M. Basic, S. W. M. Olde Damink, A. Bleich, P. H. M. Savelkoul, M. von Bergen, J. Penders, M. W. Hornef, Bile acids drive the newborn's gut microbiota maturation. *Nat. Commun.* **11**, 3692 (2020).
36. Y. Liu, J. Binz, M. J. Numerick, S. Dennis, G. Luo, B. Desai, K. I. MacKenzie, T. A. Mansfield, S. A. Kliewer, B. Goodwin, S. A. Jones, Hepatoprotection by the farnesoid X receptor

agonist GW4064 in rat models of intra- and extrahepatic cholestasis. *J. Clin. Invest.* **112**, 1678–1687 (2003).
37. M. Funabashi, T. L. Grove, M. Wang, Y. Varma, M. E. McFadden, L. C. Brown, C. Guo, S. Higginbottom, S. C. Almo, M. A. Fischbach, A metabolic pathway for bile acid dehydroxylation by the gut microbiome. *Nature* **582**, 566–570 (2020).
38. B. A. White, R. L. Lipsky, R. J. Fricke, P. B. Hylemon, Bile acid induction specificity of 7 alpha-dehydroxylase activity in an intestinal Eubacterium species. *Steroids* **35**, 103–109 (1980).
39. D. J. Parks, S. G. Blanchard, R. K. Bledsoe, G. Chandra, T. G. Consler, S. A. Kliewer, J. B. Stimmel, T. M. Willson, A. M. Zavacki, D. D. Moore, J. M. Lehmann, Bile acids: Natural ligands for an orphan nuclear receptor. *Science* **284**, 1365–1368 (1999).
40. J. Li-Hawkins, M. Gåfvels, M. Olin, E. G. Lund, U. Andersson, G. Schuster, I. Björkhem, D. W. Russell, G. Eggertsen, Cholic acid mediates negative feedback regulation of bile acid synthesis in mice. *J. Clin. Invest.* **110**, 1191–1200 (2002).
41. H. Rosen, A. Reshef, N. Maeda, A. Lippoldt, S. Shpizen, L. Triger, G. Eggertsen, I. Bjorkhem, E. Leitersdorf, Markedly reduced bile acid synthesis but maintained levels of cholesterol and vitamin D metabolites in mice with disrupted sterol 27-hydroxylase gene. *J. Biol. Chem.* **273**, 14805–14812 (1998).
42. Y. Zhang, J. Y. Hong, C. E. Rockwell, B. L. Copple, H. Jaeschke, C. D. Klaassen, Effect of bile duct ligation on bile acid composition in mouse serum and liver. *Liver Int.* **32**, 58–69 (2012).
43. Y. Matsuzaki, B. Bouscarel, T. Ikegami, A. Honda, M. Doy, S. Ceryak, S. Fukushima, S. Yoshida, J. Shoda, N. Tanaka, Selective inhibition of CYP27A1 and of chenodeoxycholic acid synthesis in cholestatic hamster liver. *Biochim. Biophys. Acta* **1588**, 139–148 (2002).
44. V. Mariotti, M. Strazzabosco, L. Fabris, D. F. Calvisi, Animal models of biliary injury and altered bile acid metabolism. *Biochim. Biophys. Acta* **1864**, 1254–1261 (2018).
45. C. Engblom, C. Pfirschke, R. Zilionis, J. Da Silva Martins, S. A. Bos, G. Courties, S. Rickelt, N. Severe, N. Baryawno, J. Faget, V. Savova, D. Zemmour, J. Kline, M. Siwicki, C. Garris, F. Pucci, H. W. Liao, Y. J. Lin, A. Newton, O. K. Yaghi, Y. Iwamoto, B. Tricot, G. R. Wojtkiewicz, M. Nahrendorf, V. Cortez-Retamozo, E. Meylan, R. O. Hynes, M. Demay, A. Klein, M. A. Bredella, D. T. Scadden, R. Weissleder, M. J. Pittet, Osteoblasts remotely supply lung tumors with cancer-promoting SiglecF^{high} neutrophils. *Science* **358**, eaal5081 (2017).
46. C. Pfirschke, C. Engblom, J. Gungabeesoon, Y. Lin, S. Rickelt, R. Zilionis, M. Messemaker, M. Siwicki, G. M. Gerhard, A. Kohl, E. Meylan, R. Weissleder, A. M. Klein, M. J. Pittet, Tumor-promoting Ly-6G^{+} SiglecF^{high} cells are mature and long-lived neutrophils. *Cell Rep.* **32**, 108164 (2020).
47. D. T. Montoro, A. L. Haber, M. Biton, V. Vinarsky, B. Lin, S. E. Birket, F. Yuan, S. Chen, H. M. Leung, J. Villoria, N. Rogel, G. Burgin, A. M. Tsankov, A. Waghray, M. Slyper, J. Waldman, L. Nguyen, D. Dionne, O. Rozenblatt-Rosen, P. R. Tata, H. Mou, M. Shivaraju, H. Bihler, M. Mense, G. J. Tearney, S. M. Rowe, J. F. Engelhardt, A. Regev, J. Rajagopal, A revised airway epithelial hierarchy includes CFTR-expressing ionocytes. *Nature* **560**, 319–324 (2018).
48. A. L. Haber, M. Biton, N. Rogel, R. H. Herbst, K. Shekhar, C. Smillie, G. Burgin, T. M. Delorey, M. R. Howitt, Y. Katz, I. Tirosh, S. Beyaz, D. Dionne, M. Zhang, R. Raychowdhury, W. S. Garrett, O. Rozenblatt-Rosen, H. N. Shi, O. Yilmaz, R. J. Xavier, A. Regev, A single-cell survey of the small intestinal epithelium. *Nature* **551**, 333–339 (2017).
49. J. L. Fachi, C. Sécca, P. B. Rodrigues, F. C. P. Mato, B. Di Luccia, J. S. Felipe, L. P. Pral, M. Rungue, V. M. Rocha, F. T. Sato, U. Sampaio, M. Clerici, H. G. Rodrigues, N. O. S. Câmara, S. R. Consonni, A. T. Vieira, S. C. Oliveira, C. R. Mackay, B. T. Layden, K. R. Bortoluci, M. Colonna, M. A. R. Vinolo, Acetate coordinates neutrophil and ILC3 responses against *C. difficile* through FFAR2. *J. Exp. Med.* **217**, jem.20190489 (2020).
50. J. Mei, Y. Liu, N. Dai, C. Hoffmann, K. M. Hudock, P. Zhang, S. H. Guttentag, J. K. Kolls, P. M. Oliver, F. D. Bushman, G. S. Worthen, Cxcr2 and Cxcl5 regulate the IL-17/G-CSF axis and neutrophil homeostasis in mice. *J. Clin. Invest.* **122**, 974–986 (2012).
51. A. R. Moschen, T. E. Adolph, R. R. Gerner, V. Wieser, H. Tilg, Lipocalin-2: A master mediator of intestinal and metabolic inflammation. *Trends Endocrinol. Metab.* **28**, 388–397 (2017).
52. C. Ryckman, K. Vandal, P. Rouleau, M. Talbot, P. A. Tessier, Proinflammatory activities of S100: Proteins S100A8, S100A9, and S100A8/A9 induce neutrophil chemotaxis and adhesion. *J. Immunol.* **170**, 3233–3242 (2003).
53. A. L. Peters, Z. Luo, J. Li, R. Mourya, Y. Wang, P. Dexheimer, P. Shivakumar, B. Aronow, J. A. Bezerra, Single cell RNA sequencing reveals regional heterogeneity of hepatobiliary innate lymphoid cells in a tissue-enriched fashion. *PLOS ONE* **14**, e0215481 (2019).
54. F. Sampaziotis, D. Muraro, O. C. Tysoe, S. Sawiak, T. E. Beach, E. M. Godfrey, S. S. Upponi, T. Brevini, B. T. Wesley, J. Garcia-Bernardo, K. Mahbubani, G. Canu, R. Gieseck III, N. L. Berntsen, V. L. Mulcahy, K. Crick, C. Fear, S. Robinson, L. Swift, L. Gambardella, J. Bargehr, D. Ortmann, S. E. Brown, A. Osnato, M. P. Murphy, G. Corbett, W. T. H. Gelson, G. F. Mells, P. Humphreys, S. E. Davies, I. Amin, P. Gibbs, S. Sinha, S. A. Teichmann, A. J. Butler, T. C. See, E. Melum, C. J. E. Watson, K. Saeb-Parsy, L. Vallier, Cholangiocyte organoids can repair bile ducts after transplantation in the human liver. *Science* **371**, 839–846 (2021).
55. L. Eckmann, M. F. Kagnoff, Intestinal mucosal responses to microbial infection. *Springer Semin. Immunopathol.* **27**, 181–196 (2005).
56. K. Atarashi, T. Tanoue, M. Ando, N. Kamada, Y. Nagano, S. Narushima, W. Suda, A. Imaoka, H. Setoyama, T. Nagamori, E. Ishikawa, T. Shima, T. Hara, S. Kado, T. Jinnohara, H. Ohno, T. Kondo, K. Toyooka, E. Watanabe, S. Yokoyama, S. Tokoro, H. Mori, Y. Noguchi, H. Morita, I. I. Ivanov, T. Sugiyama, G. Nuñez, J. G. Camp, M. Hattori, Y. Umesaki, K. Honda, Th17 cell induction by adhesion of microbes to intestinal epithelial cells. *Cell* **163**, 367–380 (2015).
57. A. L. Salzman, T. Eaves-Pyles, S. C. Linn, A. G. Denenberg, C. Szabó, Bacterial induction of inducible nitric oxide synthase in cultured human intestinal epithelial cells. *Gastroenterology* **114**, 93–102 (1998).
58. G. Kolios, N. Rooney, C. T. Murphy, D. A. Robertson, J. Westwick, Expression of inducible nitric oxide synthase activity in human colon epithelial cells: Modulation by T lymphocyte derived cytokines. *Gut* **43**, 56–63 (1998).
59. N. Molinero, L. Ruiz, C. Milani, I. Gutiérrez-Díaz, B. Sánchez, M. Mangifesta, J. Segura, I. Cambero, A. B. Campelo, C. M. García-Bernardo, A. Cabrera, J. I. Rodríguez, S. González, J. M. Rodríguez, M. Ventura, S. Delgado, A. Margolles, The human gallbladder microbiome is related to the physiological state and the biliary metabolic profile. *Microbiome* **7**, 100 (2019).
60. F. Ye, H. Shen, Z. Li, F. Meng, L. Li, J. Yang, Y. Chen, X. Bo, X. Zhang, M. Ni, Influence of the biliary system on biliary bacteria revealed by bacterial communities of the human biliary and upper digestive tracts. *PLOS ONE* **11**, e0150519 (2016).
61. H. E. Liang, R. L. Reinhardt, J. K. Bando, B. M. Sullivan, I. C. Ho, R. M. Locksley, Divergent expression patterns of IL-4 and IL-13 define unique functions in allergic immunity. *Nat. Immunol.* **13**, 58–66 (2011).
62. M. Mohrs, B. Ledermann, G. Köhler, A. Dorfmüller, A. Gessner, F. Brombacher, Differences between IL-4- and IL-4 receptor alpha-deficient mice in chronic leishmaniasis reveal a protective role for IL-13 receptor signaling. *J. Immunol.* **162**, 7302–7308 (1999).
63. P. G. Fallon, S. J. Ballantyne, N. E. Mangan, J. L. Barlow, A. Dasvarma, D. R. Hewett, A. McIlgorm, H. E. Jolin, A. N. McKenzie, Identification of an interleukin (IL)-25–dependent cell population that provides IL-4, IL-5, and IL-13 at the onset of helminth expulsion. *J. Exp. Med.* **203**, 1105–1116 (2006).
64. C. Schneider, J. Lee, S. Koga, R. R. Ricardo-Gonzalez, J. C. Nussbaum, L. K. Smith, S. A. Villeda, H. E. Liang, R. M. Locksley, Tissue-resident group 2 innate lymphoid cells differentiate by layered ontogeny and in situ perinatal priming. *Immunity* **50**, 1425–1438. e5 (2019).
65. C. E. O'Leary, X. Feng, V. S. Cortez, R. M. Locksley, C. Schneider, Interrogating the small intestine tuft Cell-ILC2 circuit using in vivo manipulations. *Curr. Protoc.* **1**, e77 (2021).
66. G. Yu, L.-G. Wang, Y. Han, Q.-Y. He, clusterProfiler: An R package for comparing biological themes among gene clusters. *OMICS* **16**, 284–287 (2012).

Acknowledgments: We thank J. Ye and members of the Institute for Human Genetics for assistance with 10X sequencing. Embryo injections were performed at the Gladstone Institutes. The UCSF Gnotobiotic Core Facility and Director J. Turnbaugh provided GF mice and performed GF experiments. The West Coast Metabolomics Core performed BA analysis. Z. Wang, M. Ji, and M. Consengco provided technical assistance. The authors acknowledge C. Lowell and A. Ma at UCSF for critical commentary. **Funding:** This work was supported by NIH grant R01AI026918 (R.M.L.), NIH grant R01HL128903 (R.M.L.), NIH grant F32 DK121476 (C.E.O.), NIH grant T32 DK007007 (C.E.O.), NIH grant F32HL140868 (M.E.K.), NIH grant T32HL007185 (M.E.K.), the Howard Hughes Medical Institute (R.M.L.), the A.P. Giannini Foundation (M.E.K.), the Diabetes Research Center (R.M.L.), the Sandler Asthma Basic Research Center (R.M.L.), Swiss National Science Foundation P300PA_171591 (C.S.), Swiss National Science Foundation P4P4PM_180832 (C.S.), the Peter Hans Hofschneider Professorship for Molecular Medicine (C.S.), and the German Research Foundation [Deutsche Forschungsgemeinschaft (DFG)] (J.S.-K.) **Author contributions:** C.E.O. planned and executed experiments, analyzed the data, and wrote the manuscript. J.S.-K. performed thick-section imaging, helped with BDL analysis, and edited the manuscript. M.E.K. performed tuft cell ablation and tamoxifen labeling and edited the manuscript. J.C.W. performed BDL surgery. A.W.S. and W.L.E. performed RNA-seq analysis. A.W.S. aided in single-cell analysis. R.R.R.-G. conceived the *Rag/Ragll2rg* experiments. J.v.M. generated the two IL-25 knock-in mouse strains and edited the manuscript. H.-E.L. generated the two IL-25 knock-in mouse strains and *Cyp8b1*$^{-/-}$ mice. J.C.d.T. performed experiments. A.B.M. planned experiments and edited the mansucript. C.S. planned experiments, aided in data interpretation, and edited the manuscript. R.M.L. planned experiments, interpreted data, and wrote the manuscript with C.E.O. **Competing interests:** The authors declare that they have no competing interests. **Data and materials availability:** The RNA-seq (GSE194035) and scRNA-seq (GSE196546) datasets are available via GEO. All other data are available in the main text or the Supplementary Materials. Requests for reagents should be directed to the corresponding author (R.M.L.).

Submitted 22 April 2021
Accepted 9 February 2022
Published 4 March 2022
10.1126/sciimmunol.abj1080

Science Immunology

Bile acid–sensitive tuft cells regulate biliary neutrophil influx

Claire E. OLeary, Julia Sbierski-Kind, Maya E. Kotas, Johanna C. Wagner, Hong-Erh Liang, Andrew W. Schroeder, Jeshua C. de Tenorio, Jakob von Moltke, Roberto R. Ricardo-Gonzalez, Walter L. Eckalbar, Ari B. Molofsky, Christoph Schneider, and Richard M. Locksley

Sci. Immunol., **7** (69), eabj1080.
DOI: 10.1126/sciimmunol.abj1080

Tuft cells monitor bile

Tuft cells are chemosensory cells located in multiple epithelial tissues that monitor their environment and activate other inflammatory cell types in response to danger signals. O'Leary *et al.* isolated biliary tract tuft cells from IL-25 reporter mice and used RNA sequencing to identify tissue-specific gene expression patterns distinguishing these cells from small intestinal tuft cells. Biliary tuft cell abundance peaked before weaning and dropped to adult levels in conjunction with increases in hepatic bile acid production. Mutant mice lacking tuft cells displayed increased neutrophilic biliary inflammation, indicating that tuft cells normally function to dampen acute inflammation in the gallbladder and biliary tract. These findings provide new insights into the tissue-specific protective functions of tuft cells residing in the biliary tract.